7-23-2015

Quantitative Study of Nano to Submicron Scales Intracellular Structural Disorder Using Electron and Confocal Microscopies: Application to Cancer Detection

Hemendra Ghimire

QUANTITATIVE STUDY OF NANO TO SUBMICRON SCALES INTRACELLULAR STRUCTURAL DISORDER USING ELECTRON AND CONFOCAL MICROSCOPIES: APPLICATION TO CANCER DETECTION

by

Hemendra Mani Ghimire

A Thesis

Submitted in Partial Fulfillment of the

Requirements for the Degree of

Master of Science

Major: Physics

The University of Memphis

August 2015

DEDICATION

I would like to dedicate this thesis to my parents Kunjar Mani Ghimire and Shobha Ghimire and my brothers Khemendra Mani Ghimire and Nabal Mani Ghimire for their love and support. I would also like to dedicate this thesis to my wife Susmita Gautam Ghimire. Without her support, this thesis would not have been possible.

ACKNOWLEDGEMENT

I would like to express my deepest appreciation to my supervisor Dr. Prabhakar Pradhan for introducing me to nanobiophotonics and cancer research. I highly appreciate his guidance and constant support throughout my research period at the University of Memphis. He has always remained a source of inspiration to focus and to be a better researcher.

My immeasurable appreciation and deepest gratitude goes to Prof. Sanjay Mishra and Prof. Mohamed Laradji for finding the time to be in my thesis committee and giving me insightful comments. My sincere thanks goes to all the professors, colleagues, and staff of the Department of Physics, University of Memphis, who have supported my research endeavors. I would like to thank Prof. R.K. Rao, Department of Physiology, and Prof. S.C Chauhan, Department of Pharmaceutical Science at The University of Tennessee, Health Science Center (UTHSC) for their collaboration and for providing biological samples to carry out the experiments, and as well as for fruitful discussions. I also acknowledge Dr. Omar Skalli, Director of the Integrated Microscopy Center (IMC), University of Memphis for providing with microscopy facilities as well as cell cultures. I am grateful to Dr. Pradeep Shukla, Dr. Sheema Sameer Khan, Ms. Lou and all the chemists, veterinarians, and technicians who contributed their expertise in my research work reported in this thesis.

Finally, I would like to thank my lab-mates Dr. Peeyush Sahay, Dr. Vibha Tripathi, and Huda Almabadi for helping me in my experimental work and computer programming. The work presented in this thesis would not have been possible without my close association with them.

ABSTRACT

Ghimire, Hemendra Mani. M.S. The University of Memphis. August, 2015. Quantitative study of nano to sub-micron scales intracellular structural disorder using electron and confocal microscopies: Application to cancer detection. Major Professor: Dr. Prabhakar Pradhan.

Cancer is one of the leading causes of death with over a million people being diagnosed every year. Many cancers eventually result in death because they go undetected in their early stages when they can be cured. The conventional techniques used for cancer diagnostics exhibit limitations in detecting early stage cancer, which has nano-scale structural changes. On the other hand, alcoholism is one of the biggest causes of health problems. This study examines the effect of alcohol in early stage carcinogenesis in the colon and healthy hippocampal cells of mice models by quantifying the structural changes in their nuclei via transmission electron microscopy (TEM). The technique utilizes the Mesoscopic Physics based concept of analyzing cellular structures by looking into their light localization properties. In a separate study, we also examined the correlation between MUC13 mucin and the tumorigenicity level in pancreatic cells via confocal microscopy imaging. The TEM and confocal images are used to construct an optical lattice system whose nano- to sub-micron scale mass density fluctuations are subsequently evaluated by statistically analyzing the spatially localized eigenfunctions of these optical lattice systems via inverse participation ratio (IPR) method. The results of TEM studies show that while the alcohol does not introduce carcinogenesis in healthy colon cells, it aggrandizes a pre-existing carcinogenesis. In hippocampal cells, alcoholism causes nanoscale morphological alterations in nuclei. The confocal studies of pancreatic cells show an existence of semblant correlation between MUC13 mucin expression and the stage of pancreatic cancer.

TABLE OF CONTENTS

LIST OF FIGURES

CHAPTER 1

INTRODUCTION

1.1 Background of the Study

Human health is one of the biggest challenges that our world is facing today. A plethora of research organizations have listed human health as their priority agenda and are spending a significant amount of time and energy for its improvement. Despite their appreciable effort, knowledge about some diseases is still in mystery. Early detection of carcinogenesis and alcohol related diseases are two prominent human health related issues that need to be thoroughly investigated. The goal of this research is early detection of carcinogenesis and alcohol related health issues in some organs by synchronizing three major components: probing device, probing site, and data analysis technique.

Microscopy techniques with suitable magnification, resolution and contrast allow us to view the physiology and biology of intracellular structures. However, the calculated selection of microscope type is imperative for all finer cytological studies. For example, general light microscopes have their limitation due to their diffraction-limited resolution (~200nm in mid visible spectra). Based on implied microscopic techniques, the work of this thesis is twofold. First, the transmission electron microscopy (TEM) has been used, so the remarkable structural complexity of the cellular nucleus is more fully revealed at higher magnifications attained with this microscopy. Secondly, conventional confocal imaging has been used for three-dimensional imaging of cells. The ability to section optically through the tissue/cells by confocal imaging is to characterize pathological changes in 4D (x, y, z, and time) makes it important for all biological studies.

Selection of probing site, particularly effected sites, in all pathological studies is equally important as probing device and analyzing techniques. Random selection of bodily sites may be less worthy for the accurate estimation of disease level. For example, to study the first effect of ethanol feeding in mice, one should check alteration in sense of brain, heartbeat, respiratory action or any other bodily systems, which shows immediate response or long-term effects of alcohol consumptions. For this cytological study, morphological alteration in the cell nuclei of the effected region is critical because a nucleus is the site in a cell where DNA is housed and where the process of cellular response against toxicity of external stimuli begins. The nucleus is now known to be the repository of the genome and the source of the informational macromolecules that control the cellular function.

Moreover, a visual inspection of microscopic cellular images has been often insufficient to detect the important morphological alteration; a quantitative analysis of cellular morphology is required for an accurate estimation of the changes. Despites earlier efforts, the quantitative information imbedded in the TEM images and confocal images of a biological cell has not been properly understood until recently. In this project, the light localization property of biological cell has been used to obtain quantified values of nano- to sub-micron scales morphological alteration in prominent intracellular mass due to progress of carcinogenesis, toxicity effect due to the consumption of alcohol as well as combine effect of carcinogenesis and consumption alcohol have been studied.. Light localization technique of optical lattice systems derived from TEM and confocal microscopic imaging, which takes care of heterogeneity nature of medium, is one of the efficient techniques for structural/morphological analysis.

1.1.1 Nuclear structure

The nucleus is the control center of biological cell, which regulates the integrity of genes and gene expression [1]. Acting like the brain of the biological cell, the nucleus is responsible for protein synthesis, transportation and other important cellular functions. The majority of a cell's genetic materials is stored in the nucleus and is in the form of organized structural components called chromosomes. Arrangement of chromosomes along with other components such as nuclear membrane, nucleoplasm and nucleolus, determines the biomechanics, biochemistry and hence morphology of the nucleus [2].

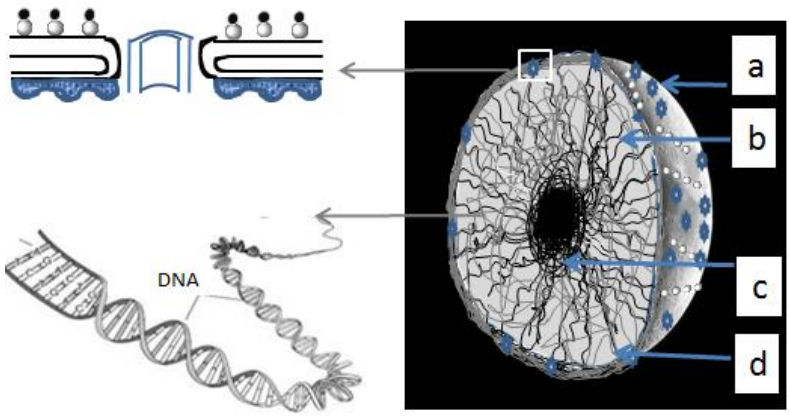

Fig. 1.1.Well-labeled nuclear structure: (a) Nuclear envelope composed of two membranes with embedded nuclear pores, (b) Chromosomes, (c) Nucleolus, (d) Nucleoplasm.

The arrangements of important nuclear components responsible for the nuclear structural architecture are as shown in Fig. 1.1. The nuclear envelope is a highly specialized biological interface composed of two membranes with embedded nuclear pores, and it plays an important role for the coordination of gene action or transport of material between nucleus and cytoplasm. The outer nuclear membrane is contiguous with

the endoplasmic reticulum (not shown in figure), and underlying inner nuclear membrane is attached to the protein meshwork nuclear lamina, which provides support for nuclear envelope and anchors other macromolecules [3]. The packages of genes and protein like threads pointed by the arrow (b) in Fig. 1.1 are chromosomes. These unique structures of DNA tightly wrapped around histones are important for cellular function and genetic transformation. As the largest structure in the nucleus, composed of proteins and RNA, the nucleolus is surrounded by a chromosomal region and serves as the site for ribosome synthesis and assembly. Permeating the chromosomes and nucleoli, the highly viscous fluid enveloped by the nuclear membrane is nucleoplasm, which dissolves substances like nucleotides (for replication of DNA), enzymes (for activities in nucleus) and soluble liquids (nucleosol) are dissolved in nucleoplasm [4].

1.1.2 Nuclear morphological characterization

What will happen to the performance and spatial arrangement of nuclear macromolecules, when a healthy cell is in contact with external stimulus like disease, drugs or radiations? Nuclear macromolecules will start to rearrange due to presence of toxicity in these external stimuli. It is now recognized that beyond a certain level, these stimuli could disrupt the biological rhythm, which would lead to an alternation in the chemical or mechanical performance and hence morphology of the nucleus [5]. The morphological characterization of respective organelles, cells, or tissues is important for biomedical applications [6]. Significant morphological studies include early cancer detection [7,8,9], cell division, proliferation, transition and apoptosis [10,11], study of environmental stress [12].

Oncological studies have shown that the degree of disease-induced nuclear morphological changes is always proportional to the level of malignancy and that becomes the hallmark of the advances in cancer detection and treatment [13,14]. We have several evidences to verify the alteration of the nano-architectural changes in a cell that results into the increased of the nanoscale spatial mass-density fluctuations with the progression of carcinogenesis. Partial-wave spectroscopic and TEM studies have shown that the enhancement level in nanoscale fluctuations in the morphology of nuclear components that could reflect into nanoscale spatial density fluctuation along with the initiation and progression of carcinogenesis [15].

Advances in understanding the morphological alteration in nuclear structures due to malignancy have also revealed insights about the detection and treatment of carcinogenesis. Therefore, we have now a plethora of biomedical applications of morphological studies (by segmentation, localization, estimation, modeling, shape analysis and so forth) to extract intracellular abnormalities in specific nuclear component. However, in this era of personalized medicine, the manual segmentation of cellular components and measurement of size/shape from microscopic images are very labor-intensive and even infeasible. The morphological alteration, reflected as the nanoscale spatial mass density fluctuation in the bulk nuclear mass, could be an efficient way for nuclear morphological studies. This level of spatial mass-density fluctuation becomes easily noticeable by using existing pathological techniques at the advanced stages of external stimuli such as carcinogenesis, but present technologies have failed to detect changes at early stages [16,17].

1.1.3 Nanoscale disorder quantification

Visual inspection of microscopic images is sufficient to estimate the drastic morphological changes in biological cells, but fails to distinguish important nanoscale to sub-micron scales of changes. To adequately detect and characterize such small scales of morphological changes, quantitative assessment of morphological disorder at the nanoscale, i.e., the degree of nanoscale structural disorder is required [18]. The quantitative evaluation of subtle changes in nuclear morphology, which is important for the precise characterization of cytological disorder associated with specific diseases, has recently been a major research interest. [19].

However, it is not easy to develop such a robust technique that can precisely quantify the important atomic or molecular level of alteration that researchers can use to distinguish the most important intracellular features. Different avenue to the disorder quantification is inevitable, when intracellular changes needed to be measured are very small, in the order of nano- to micrometer. Assuming biological cells as weakly disordered dielectric optical media and by using the light scattering/localization properties, one can make the quantitative analysis of structural disorder in biological cells. Due to multiple interference effects, from the disorder structure, light wave is localized in a disorder media. The light localization technique can characterize the heterogeneous nature of biological cells, and can overcome the difficulties associated with the earlier techniques.

Similar as a localized wave function of electrons in disordered solids, light also shows localization properties in the biological medium (i.e. disordered dielectric media) [20]. Anderson’s light localization properties of disordered optical/dielectric media have

been thoroughly studied in Condensed Matter Physics and numerous investigations have been made in underlying physics behind disordered lattice systems [21,22]. In our cytological studies, light localization properties of the cellular nuclei are investigated by constructing disordered optical lattices constructed from both TEM and confocal imaging, and statistically analyzing the localization properties eigenfunctions of these lattices via the inverse participation ratio (IPR) technique. The advantage of this technique is that this provides the statistical quantities such as means and standard deviations of these IPR values at the given sample length gives the quantitative measurement of disorder in a single parameter.

1.2 Problem Statement

Detailed evidence reported by the World Health Organization (WHO) shows that public awareness programs related to the use of alcohol and carcinogenesis are always listed in the world's priority agendas [23]. It is not surprising that a significantly large portion of intellectual minds and the world's economy are allocated to cancer and alcohol-related research [24]. However, we are still lacking sophisticated technologies that can detect the nanoscales of morphological disorder in the biological media. In this thesis, we have used several advanced Condensed Matter Physics concepts and techniques, and conventional microscopic techniques to measure and analyze nanoscale to sub-micron scales of morphological alteration in the nuclei of colon cells, hippocampal cells and pancreatic cells due to carcinogenesis and the effect of alcoholism. We found that nanoscale morphological analysis gives quantified values of structural alterations before the alteration become evident to existing tools.

The WHO 2014 report shows that more than 200 human diseases are linked with alcohol consumption [25]. The primary diseases associated with alcohol consumption are anemia, cancer, cardiovascular disease, cirrhosis, dementia, depression, gout, seizures, high blood pressure, infectious disease, nerve damage, and pancreatitis. Furthermore, more than 86 percent of people ages 18 or older report that they have drunk alcohol at once some point in their lifetime and one third of this percent are currently engaged in heavy drinking. The National Institute of Alcohol Abuse and Alcoholism (NIAAA)'s report on the same issue matches with WHO statistics. Therefore, psychoactive drug alcohol that has been widely used as a social lubricant in the sense of happiness is now becoming a threat to the global health issues.

In addition to the foregoing complications of alcoholism, carcinogenesis also presently remains as one of the most challenging health issues for the century [26]. Based on National Institute of Health (NIH) data, approximately 39.6 percent of men and women will be diagnosed with cancer at some point during their lifetimes (from 2010-2012 data) and the number of new cases of cancer (cancer incidence) is 454.4 per 100000 men and women per year (from 2008-2012 cases). Therefore, the early diagnosis of cancer should be a primary goal for every government and research organization. Because most cancers are curable if diagnosed earlier, and there is of less chance that treatment will be curative if cancer reaches to more advance form and spreads metastasis.

To resolve these health issues, studies of atomic or molecular-level changes in the biological cell are more effective than macroscopic studies. Similar to the assessment of risk of cancer at the atomic level, alcohol is itself a chemical disease, which breaks down differently at the same level. There is a plethora of research that attempts to explore

nanolevel architectural interrogation in the cellular nucleus for the prognosis of early stage carcinogenesis [27]. These studies show that carcinogenesis and chronic alcoholism effects are organ specific, and result in the rearrangement of nuclear macromolecules. The degree of molecular rearrangement depends on the level of malignancy and cellular type, so the nanoscale fluctuations in the nuclear morphology and hence spatial fluctuation in mass density is amplified with the enhancement in the level of alcoholism or carcinogenicity [28,29].

1.3 Research Objectives

In a broader picture, the main goal of this research is to develop efficient technique, using advanced Physics methods in understanding the progress of carcinogenesis and added drug at the cellular level, by quantifying the spatial mass density fluctuations in the cell nuclei. For this, we have used TEM and confocal microscopy imaging modalities, and developed a technique to quantify the changes in the nano- to sub-micron scale structural disorder in cellular nuclei due to carcinogenesis, alcoholism and due to combine effect of alcoholism and carcinogenesis in different bodily sites. To be more specific, main objectives of this study are the following:

- **Development of technique to quantify the structural disorder in cell nuclei**

Using the mesoscopic light transport properties of biological cells, we have developed technique to quantify the nano-to-submicron scales structural disorder in cell nuclei using TEM and confocal imaging of this cell. In particular, the structural disorders are obtained via the light localization properties of these biological cells. Our developed technique have advantage to understand the disease level with great precision, before change becomes evident to visual inspection of microscopic images.

- **Study of aggravation effect of chronic alcoholism of early colon carcinogenesis using TEM**

Recent studies on aggravation effect of excessive alcohol consumption for the initiation and progression of colon cancer show that progression of carcinogenesis is associated with intracellular morphological events, DNA repair, folate/alcohol metabolism, and genetic alteration at the molecular level. Those studies have achieved a new paradigm of understanding the respective tumorigenesis. However, there is no efficient technique to establish an association between alcohol consumption and multiple genetic and epigenetic alterations during colon cancer progression. In this study, using our quantification technique, we compare the morphological fluctuation at the nanoscale reflected by the spatial nanoscale mass density fluctuations present in the nuclei of early carcinogenic colon cells in mice cancer model, administered with or without alcohol.

- **Study of early detection of neurological disorder in hippocampal mass due to chronic alcoholism using TEM**

Previous investigations on neuropathology suggested that excessive consumption of alcohol results in significant hippocampal neuro-degeneration. Studies with a common pathological device like the white light microscopy and the magnetic resonance imaging (MRI) technique showed that chronic alcoholism leads to morphological alterations in tissues followed by minor losses in hippocampal volume. However, there is no remarkable quantitative evidence to associate alcoholism and its intracellular morphological alteration when changes are of nanoscale or molecular levels, in early alcoholism. By using our developed technique, we have experimentally studied the effect of chronic alcoholism on hippocampal cellular nucleus.

- **Study of treatment approach for early pancreatic cancer by altering MUC13 protein**

The pancreas is deep inside the body, so the symptoms of pancreatic cancer may not be evident according to recent pathological techniques until it reaches its advanced stages. Once it is diagnosed, pancreatic cancer is very hard to control. In addition, the complete surgical removal of the carcinogenic pancreas, which is the primary source of digestive juices and hormones that regulate blood sugar, is impossible. Thus, it is imperative to have advanced pathological techniques for the early diagnosis and treatment of pancreatic cancer. Here, we have studied the malignant stages of colon cancer by associating the level of MUC13 protein expression (or suppression) in epithelial pancreatic mass with the metastatic phenotype of pancreatic cancer by quantifying their light localization property at submicron length scales.

1.4 Scope and Limitations of Study

In this study, we have used transverse light localization property in disordered optical lattice system created from TEM and confocal microscopic imaging of biological cells to analyze important morphological alterations from nano to sub-micron scales in the cell nuclei. The technique we have used is based on Mesoscopic Physics concepts for the quantification of structural disorder and the technique has potential application for early cancer detection. Preliminary results are encouraging for precise disorder quantification earlier than it becomes evident to recent pathological tools.

The mentioned robust technique has been implemented to achieve nanoscale changes in nuclei of colon cells, hippocampal cells and pancreatic cells with different disease conditions, as well as with the effect of drugs. The preliminary results have

provided us with the quantified values of spatial disorder/fluctuations in the nuclear mass density, before this disorder/fluctuation becomes evident from the visual inspection of microscopic images. Therefore, this approach is not only good for early detection of morphological alteration, but also good for achieving a new avenue for disease analysis by helping existing pathological techniques.

To be more specific, the abovementioned technique is implemented with the following microscopies and disease conditions.

- *Transmission Electron Microscopy (TEM)*:

  (a) To probe the effect of chronic alcoholism on intracellular morphological alteration during the early stage of colon carcinogenesis.

  (b) To probe the effect of chronic alcoholism on intracellular morphological alteration in the hippocampal cell nuclei.

- *Confocal Microscopy*:

  Quantification of morphological alteration in sub-micron scales of the pancreatic cellular nucleus reflected as alteration in levels of MUC13 expression.

Although this research was carefully prepared, we are still aware of its limitations and shortcomings.

1. This study is limited to a mice model. First, the number of chromosomes and intracellular structure of the mice cells and human cells are different. Therefore, we have to be aware of these factors before generalizing it in human studies.
2. TEM experiments are difficult to be implemented in everyday pathological application. Sample preparation of TEM and imaging is time consuming and requires

certain expertise. Therefore, its implementation will be limited to few research laboratory and hospitals.

3. This study is limited to one level of carcinogenesis. If we are able to create a organ specific universal calibration curve for different levels of carcinogenesis, our research will be more pragmatic and could potentially save millions of lives.

1.5 Literature Review

In our literature review, we have had good representative of literatures discussing about the nuclear morphological alteration due to diseases, drugs, and cellular functions. A vast amount of publications has reported the use of the morphological cell analysis method in bio-informatics and biomedical research. They have used alteration in cell morphology as a standard diagnostic or prognostic biomarker in dealing with cancerous and precancerous cases. However, their approaches of analysis were suitable only for the later stages of cellular aggravation and only little information is mentioned about the early stage morphological changes associate with cancer. The relevant academic journals, highlights, warnings and commercials that have important achievement in the following cases are included in our review.

(a). The usage of intracellular morphological alteration during the early stage of carcinogenesis as a biomarker to study the progression of cancer with/without external stimulants (primarily alcoholism).

(b). The association between alcoholism/neurological disorder and the dimensional alteration in hippocampal mass.

(c). Pancreatic cancer diagnosis and treatment by using MUC13 mucin expression in pancreatic adenocarcinomas as a biomarker.

- **Literature on cancer initiation and progression**

A person does not go suddenly from being healthy to having cancer. Cancer in the present day is the result of genetic predisposition or cancer-causing behaviors from the past few years. The development of cancer usually takes several years to decades to form and numerous atomic to molecular changes occur from the time of its initiation to the time of its detection [30,31]. The pace at which cancer grows and spreads depends on the patients' health condition, external environment and level of carcinogenesis.

There are more chances of regaining initial health by curing the disease, if the malignant condition is diagnosed early. Therefore, in this era of personalized medical therapies, scientists have developed several screening tests, therapeutic studies, chemical, optical, magnetic, morphological and other tests [32]. Recent spectroscopic microscopy studies have shown that spatial fluctuation in intracellular morphology increases with an increase in the level of carcinogenesis [33,34,35]. At the earlier phase of malignancy, cellular morphological alteration is very small, so the alteration could be easily concealed from present pathologists. As the level of disease increases, the degree of morphological alteration also increases and would be evident to present diagnostic techniques [36].

- **Literature on cancer and alcoholism**

Factors such as genetic predispositions and external environment of the past years unmistakably contribute to present health [37]. Miller Bruce, an American nutrition specialist, highlighted some cancer causing behaviors and environmental factors in his book *Cancer: We Can Win the War against Cancer* "by aggressively pursuing prevention". Chronic consumption of alcohol, an antagonist of the methyl group metabolism, was shown to be related to DNA methylation and further to the progression

of colon cancer [38,39]. Amount of folate in blood or tissue plays an important role in DNA synthesis and methylation. Folate deficiency could lead to the alteration in the methylation pattern; this, in turn, could change genetic and epigenetic performance.

- **Literature on alcoholism and neurological disorder**

The immediate effect of alcohol is an alteration in the brain's perception followed by the dysfunction of other organs [40]. Chronic alcoholism interferes with the transformation of data from the short-term memory to the long-term memory. The pathological techniques, such as magnetic resonance imaging (MRI) and light microscopy (Golgi's method) studies for neurological disorder have shown that chronic alcoholism could alter the morphology of the hippocampus [41 , 42]. Although the hippocampus, which is very susceptible to adverse effects of alcohol use, can serve as the quantifiable marker for the alteration in brain function, the existing techniques could not detect when changes happened at an early stage [43, 44,45,46].

- **Literature on MUC13 protein alteration and pancreatic cancer progression**

Pancreatic cancer is one of the most deadly malignancies in humans with a poor prognosis. In previous studies, MUC13 transmembrane mucin expression in pancreatic cancer, similar to other families of carcinogenesis (ovarian, gastric and colorectal), is used as the biomarker to determine the level of malignancy [47]. This association between the level of MUC13 transmembane mucin expression and the molecular mechanism of pancreatic cancer can offer a new avenue for cancer prevention and treatment.

- **Rationale**

Based on the literature review, we have proposed the cytological study for the nano to submicron scale of morphological alteration in the nuclear nano-architecture reflected as the spatial density fluctuation in nucleus due to malignancy. Nano- to sub-micron scales of morphological alteration in the biological changes are not palpable to the existing pathological techniques and the disease does not show its symptoms for many years. Detecting cancer diseases via present pathology followed by observation of other bodily symptoms decreases the chances of curing, because there are more chances of cancer spreading to blood streams and lymph nodes for metastasis. Similarly detecting the neurological damage after dimensional alteration in the hippocampal mass could lead to alteration in brain functions. Therefore, analysis of nano to submicron scale of morphological alteration could diagnose the malignant levels in their early stages.

In the proposed cytological studies associated with effect of alcoholism in cellular mass of normal hippocampus cells and colon cells with different level of carcinogenesis have been quantified. Literature shows that cellular functions such as, DNA repair, folate/alcohol metabolism and genetic/epigenetic modification alters due to alcoholism [48,49]. Furthermore, oncological studies show cancer progression involves the genetic and epigenetic modification [50]. The colon stores the consumed chemicals and drugs before removing through stool, and billions of bacteria coat the colon and its contents [51,52]. Similarly, chronic alcoholism leads to histopathological changes in the nervous system [53]. These are the reasons why we have analyzed effect of alcoholism for the nanoscale of morphological alteration in the hippocampal cellular nucleus and colon cell nucleus with different level of carcinogenesis.

Similarly, another proposed cytological study in this thesis is MUC13 mucin expression and pancreatic cancer level. Literature shows mucin expression has proportional relation with the pancreatic cancer level when it is in progressive stage [54]. The reason why we studied this is to check whether the sub-micron scale of morphological alteration decreases along with the reduction of mucin expression via different therapeutic approaches. We have borrowed advanced Condensed Matter Physics concepts to analyze the nanoscale level of disorder in the biological cells, so this method could have the potential for pancreatic cancer diagnosis and treatment.

1.6 Organization of the Thesis

This thesis report presents the technique of nano to sub-micron scales of morphological alteration in the nucleus of the colon cells, pancreatic cells and hippocampal cells due to progressive carcinogenesis and change of these progressions due to alcoholism. In this thesis, we have included important theoretical/experimental evidences from previous researchers, implied techniques outcomes, and their importance for the possible improvement of people's health and well-being. Concisely, the report is organized in the following manner:

Chapter-1 is introduction and it is divided into four parts; the first part of this chapter is background: basic principles of probing signal, site, and analyzing technique of our studies are outlined. The second part of this chapter provides broader prospective of this project. The third part outlines the important scopes or weakness and the final part address overview of previous research (literature review).

Chapter-2 provides the experimental TEM and confocal methods and corresponding data analysis technique of this study. We have included theoretical explanation behind each

technique, which provides information about concepts, assumptions and theories that support this research. In particular, for the data analysis technique we have discussed the quantification of nanoscale structural disorder of biological cells using the light localization properties of these cells via inverse participation ratio (IPR) method.

Chapter-3 presents the result of our work based on the developed techniques in Chapter 2. This section is divided into two parts. In the first part, we present the result on TEM studies of the effect of alcoholism in colon cancer initiation and progression, and effect of alcoholism for neurological disorder in mice model. In the second part, we report the quantitative association of MUC13 mucin with level of pancreatic carcinogenesis in cultured cell lines derived from human patient via confocal microscopy studies.

Chapter-4 is the conclusion section; we discuss the potential applications and offers recommendations for improvements to this work.

CHAPTER 2

MODELS AND METHODS

This chapter deals with the detailed description of animal models, chemical administration and animal preparation, probing devices selection, device calibration, sample preparation, and images (data) analysis techniques. The experimental study was done by using mice cancer model and cultured human cancer cell lines. Biological specimens derived from mice models and human cancer cell lines are imaged via TEM and confocal microscopy techniques. Based on implied microscopic techniques, in particular transmission electron microscopy (TEM) and florescence confocal microscopy, sample preparation, signal-sample interaction and disordered optical lattice system construction processes were divided into two-folds.

2.1 Animal Model

Mice models have been used extensively for studying various human diseases [55]. Mice have similar anatomy, physiology, and genetics as humans, and are cost effective (small patient size, less generation time, accelerated life spans), therefore, mice models are popular in most bacteriology. The effect of biological disease (cancer) or chemical diseases (alcohol) in this study has a direct relation to genetic and epigenetic modifications. Therefore, a mice colon cancer model, in particular azoxymethane (AOM) treated mice (AOM-mice) model with similar genome to that of human is the best option to see the effect of chronic alcoholism in colon cancer progression and hippocampal neurological disorder. Further treatment with dextran sodium sulfate (DSS) induces colitis and makes the overall colon cancer growth more efficient than only AOM-mice colon cancer model. We have used C56BL6 female mice (AOM, DSS, LieberDeCarli

chemical administered) in the above-mentioned two cases. In second case, preliminary study of diseases like pancreatic cancer is also possible via cell culture of pancreatic cancer cell lines. Cultured cells of pancreatic cell lines have been used to associate the level of MUC13 protein expression (or suppression) in epithelial pancreatic mass with the metastatic phenotype of pancreatic cancer.

2.1.1 Laboratory mice preparation and chemical administration

We have studied the aggravation effect of alcohol in early colon cancer and hippocampal morphology in adult (10-12 weeks) female C57BL6 mice. The experimental time starts from the day of putting tags for these mice identifications. On the day zero of these experiments, we caged mice with three mice per cage. The mice are divided into four categories for following sets: (i) control mice, (ii) alcohol treated mice, i.e., Control+EA, (iii) AOM/DSS treated mice, (iv) AOM/DSS-mice treated with alcohol or AOM/DSS+EA. (i) For control mice model, only saline injections were provided. (ii) For alcoholic mice model, other than saline injection as described in (i), ethanol liquid diet (LieberDeCarli liquid diet with 4 percent ethanol) is provided form the day 10 to next 15 days (10 to 25 day). Additional ethanol ingestion was introduced from day 31- day 44. (iii) For AOM/DSS-mice model, a single dose (intraperitoneal injection) of azoxymethane (AOM) with 10 mg/Kg body weight was provided on the zero days. From day 1 to day 4, mice are in rest, and from day 5 to day 9, mice are in first cycle of dextran sodium sulfate (DSS). 250 ml water with 3 percent DSS is put in a can three times in the 5 days period and allow mice to ingest fully (i.e. one mice will get approximately 150 ml of water and 5 ml of DSS in first cycle of DSS ingestion). DSS induces colitis, which results in severe diarrhea bleeding and hence loss of body weight. We repeated the same

procedure for the second cycle of DSS ingestion (day 25-30). (iv) For AOM/DSS-mice with alcohol (EA) model, the AOM/DSS treatments was same as described in (iii), Additionally, on the day 10, mice were fed with ethanol liquid diet (LieberDeCarli liquid diet with 4 percent ethanol) until the next 15 days. Further ethanol ingestion was introduced from day 31 to day 44. This diet allows for the prolonged exposure of ethanol in a rodent model. Note: Administration of ethanol in a nutritionally adequate gel (LieberDeCarli liquid diet with 4% ethanol) provides a simple method for studies on chronic ethanol effects in rodents.

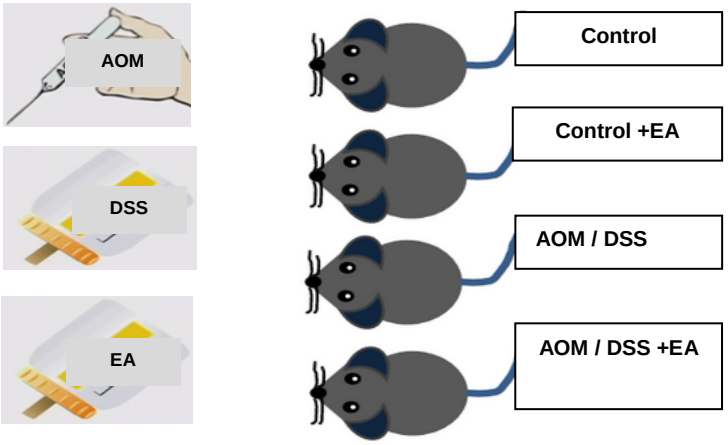

Fig. 2.1. Mice models for TEM study: normal, alcoholic, early colon carcinogenic, alcoholic with early colon carcinogenic.

On the day 45 of AOM ingestion, we have four groups of mice as shown in Fig. 2.1. The (i) first group consists of normal mice (Control), (ii) second group have chronic alcoholic mice (Control+EA), (iii) third group have early colon carcinogenic (AOM/DSS), and (iv) last groups, have early colon carcinogenic with chronic alcoholism (AOM/DSS+EA). These four groups of mice were raised and were sacrificed in

collaboration with well-trained and licensed experts. Colon and hippocampal biopsy samples thus obtained from three members of each groups were preserved in different containers and further processed for transmission electron microscopy imaging using a standard protocol as described in later section.

2.1.2 Human pancreatic cell line culture

To establish an association between level of MUC13 protein expression (or suppression) with the metastatic phenotype of pancreatic cancer, we have used the pancreatic cancerous cell lines derived from human pancreatic cancer. Discussed pancreatic cancer types include:

(a) AsPC-1 pancreatic cancer cell lines (adenocarcinoma of the head of the pancreas and metastases to several abdominal organs [56]),

(b) BxPC-3 pancreatic cancer cell lines (adenocarcinoma of the body of pancreas and no metastasis [57]),

(c) Panc-1 pancreatic cancer cell lines (adenocarcinoma of the head of pancreas that invaded duodenal wall and metastasis in one peri-pancreatic lymph node [58]), and

(d) HPAF pancreatic cancer cell lines (adenocarcinoma and metastases pancreatic cells to liver, diaphragm and lymph nodes [59]).

Human pancreatic cancer cell lines are acquired from the American Type Cell Culture Collection were maintained at 37^{o}C and grown in the recommended medium and followed the protocols to maintain the authenticity of the cell lines. The intracellular morphological alteration from each type of pancreatic cancer is evident to existing pathological microscopy. Thus, cultured cells were stained with suitable dye for confocal microscopy.

2.2 Selection of Probing Devices

To investigate certain aspects of cell structures, cytologists and histologists utilize different microscopic techniques. The selection of microscope depends on the nature of the probing site and nature of study. Light microscopes phase contrast microscope, interference microscope, polarization microscope, fluorescent microscope are used to examine some structural details of individual tissue or cells and a thorough knowledge of intracellular morphology can be obtained via electron microscopies. Selected microscopies for our study are as follows:

2.2.1 Transmission electron microscopy

To understand the earlier initiating morphological events in diseased cells is critical and requires the ability to detect scales less than a micron. Spectral optical microscopy studies have suggested that early stages of diseases like carcinogenesis involve mass-density fluctuation approximately 10-100 nm, which is identical to the length scale of cellular building blocks (e.g. DNA, RNA, proteins, and lipids). Conventional visible light microscopy has been widely used to characterize biological systems (cells and tissue) at the later stage of diseases that involves accumulation of multiple genetic and epigenetic alterations, resulting in morphological changes at the micron and supra-micron scales. However, the ability of these pathological microscopy techniques to detect at nanoscale is restricted by their diffraction-limited resolution. Diffraction limit of such pathological bright field light microscopy is about 200 nm resolution in mid-visible light and useful magnification is below 2000x [60]. This difficulty led us to explore the potential of transmission electron microscopy (TEM), with its significantly higher resolution for early detection of disease.

Basic principle of TEM

The instrument alignment of TEM is as shown in Fig.2.2. It is composed of several components, which includes a vacuum system, specimen stage, electron gun, electromagnetic lenses (condenser, objective) and apertures. The source of illumination, electron beams of very short wavelength are emitted from the electron gun at the top of an evacuated chamber and travel through the vacuum to avoid the collision of electrons with air molecules and hence scattering of electrons. Just like glass lenses placed in light microscopy, magnetic coils are placed in specific intervals, which worked as electromagnetic condenser lens system to focus the electron beam on the specimen. When the incident electrons pass through the specimen stained with an electron dense material, these are scattered by the internal electron charge densities. Scattered electrons are magnified and collected to the phosphorescent screen or to the charged coupled device (CCD) via electromagnetic objective, intermediate and projector lenses.Based on the alignments of components, the working of TEM is divided into three sections [61].

Illumination system: The part of TEM above the specimen, which includes an electron gun and condensers, belongs to the illumination system. It illuminates the specimen by high-energy beams of electrons coming out from the electron gun. If we maintain the potential drop V between filament and anode, electrons will gain the kinetic energy and momentum as follows:

$$K.E = eV = \frac{mv^2}{2} \qquad \text{…..... (2.1)}$$

$$P = mv = \sqrt{2meV} \qquad \text{..... (2.2)}$$

where, *m*: rest mass of an electron = 9.1 x 10^{-31} Kg and *e*: charge of an electron = 1.6 x 10^{-19}C. Substituting these information in de-Broglie's wavelength in terms of Planck's constant *h* = 6.63 x 10-34 m^2Kg/sec. The wavelength of electron for non-relativistic case, (potential < 100V) is;

$$\lambda(A^o) = \frac{h}{P} = \frac{h}{[2meV]^{1/2}} = \frac{12.27A^o\sqrt{volts}}{\sqrt{V(volts)}} \quad \text{..... (2.3)}$$

Similarly, when the driving potential is more than 100V, the velocity of electrons becomes greater than half the velocity of light, we should consider relativistic case, and wavelength of electrons is;

$$\lambda = \frac{h}{P} = \frac{h}{\left[2meV(1+\frac{eV}{2mc^2})\right]^{1/2}} \quad \text{..... (2.4)}$$

The objective lens and stage: This combination is the heart for TEM, which limits the resolution. To find the resolution of TEM, substituting value of wavelength λ from above equation to Abbe's equation;

$$d_{TEM}(A^o) = \frac{0.61\lambda}{n*\sin\alpha} = \frac{7.53A^o\sqrt{volts}}{\alpha\sqrt{V(volts)}} \quad \text{..... (2.5)}$$

Imaging system: It includes the intermediate lens, projector lens and CCD (not shown in figure). In this system image formed is further magnified by a series of magnetic lenses until it is recorded by hitting a light sensitive sensor then finally to computer screen.

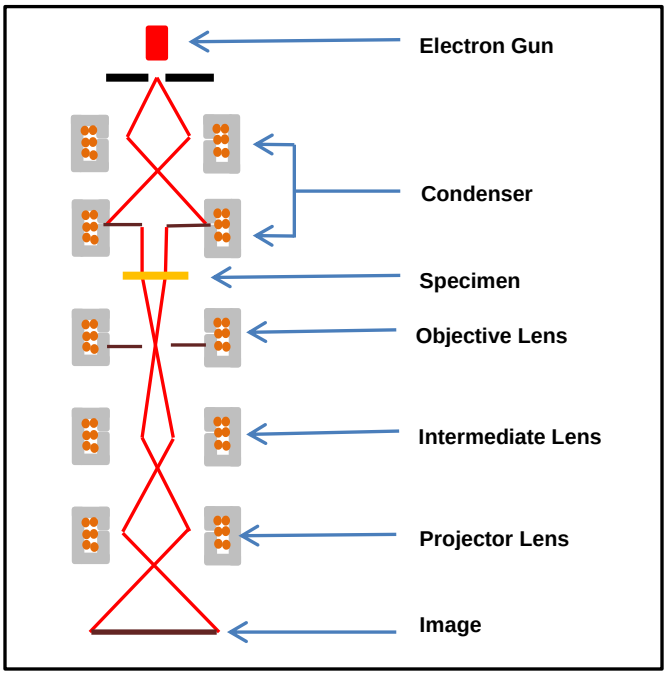

Fig. 2.2. Schematic diagram of TEM: with labeled illumination, resolution and imaging components.

Sample preparation for TEM Imaging

The sample preparation of biological tissue for TEM imaging should address the problematic features such as requirement of vacuum, sample size, contrast and conductivity. The high water content of biological specimen makes it difficult to restore the structure in vacuum. Biological specimen is placed in the vacuum chamber while TEM imaging. The necessary sample thickness is often much smaller than the thickness of a cell, slicing biological tissue that thin is problematic and the biological tissue has very low electron density, which results into few electron scattering events and low contrast images. In addition, the samples are generally nonconductive and there are more chances of distortion of images due to probing electrons. Structurally weak, hydrated and electron translucent features of biological media are exactly opposite to what is required

for TEM imaging. Therefore, we have followed all of the following necessary procedures for sample preparation, so that our specimen becomes suitable for TEM imaging.

Fixation- A biopsy sample (colon or hippocampal) extracted from each kind of treated animal subset were primarily fixed in 0.1 M Na cacodylate buffer (pH 7.2 to 7.4) containing 2.5 percent glutar-aldehyde and 2.5 percent paraformaldehyde, for more than two hours. These fixed samples were then cut into small cubical shapes by using two razor blades without deforming tissue and were transferred to a second glutar-aldehyde solution. Then, specimen is washed (10 min x 3 times) with several changes of 0.1 M cacodylate buffer (pH 7.2 to 7.4) to preserve structure. We post fixed this sample with 2 percent osmium (OsO_4) in 0.1 M Na cacodylate buffer for 1-2 hours (4^oC) and rinsed it with several changes of 0.1 M cacodylate buffer (pH 7.2- 7.4), which helps us to fix lipid molecules.

Dehydration- Following the standard protocol, samples were En-Block stained with aqueous UA and dehydrated through the series of ethanol (50%, 70%, 80%, 90%, 95%, 100%, and 100%) for every 15 minutes, after rinsing it with deionized water.

Embedding and polymerization- Sample is embedded in polymer resin containing Epon to stabilize them sufficiently to allow ultrathin sectioning followed by polymerization at 35^oC 1day, 45^oC 1 day and 60^oC 1 day.

Trimming and sectioning- Thoroughly cleaned and concentrated samples prepared above were then trimmed to one mm square shape and were further sectioned with an ultra-microtone to thickness of 70 nm, so that our sample will be electron transparent and mechanically robust.

Staining- Ultrathin specimen were fixed in grating grids and stained with the Uranyl acetate (stains nucleic acids) and lead citrate (stains protein and glycogen granules). The specimen is now extremely thin for highly absorbable electrons to penetrate and is ready.

Calibration of TEM setup

In this TEM study, we have used Joel JEM-1200 transmission electron microscopy fitted with Hamamatsu ORCA HR camera at 810 Exposure, 2 Gain and 1 Bin, for the imaging system. Sample holder is first sanitized and the mechanically robust dehydrated specimen is fixed in the sample holder and is scanned by illuminated electron beams at 60 KeV and images were recorded. In the first project, early detection colon cancer (alcoholism and colon cancer progression for mice models), we have fixed magnification 6000x and all other physical parameters were constant. We have analyzed n=15 TEM micrographs (from 3 mice per set, 5 micrographs per mice) from the nuclear region of colon cells derived form of each types of treat mice (3 mice per type): (i) Normal (Control), (ii) Alcoholic normal (Control + EA), (iii) Early colon carcinogenesis (AOM/DSS) (iv) Alcoholic mice with early colon carcinogenesis (AOM/DSS + EA). Similarly, for the second TEM project, alcoholism and neurological disorder, by using magnification 3000x and other calibration scales same as previous work, we have taken n = 15 (from 3 mice per set, 5 micrographs per mice) micrographs from the nuclear regions of the cells from hippocampus of each set: (i) Normal and (ii) Alcoholic.

2.2.2 Confocal microscopy

Confocal microscopy is an integrated optical technology that combines the optical and digital image analysis technique to provide three-dimensional voxel imaging of biological samples. The specimen is scanned with the help of point source and reflected

beam is filtered via pinhole, which rejects out-of-focus light. Suppression of signals coming from out of focus planes and accomplish 3D resolution with the help of the pinhole is an important feature of confocal microscopy, which makes it popular in most of biological studies.

Basic principle of confocal microscopy

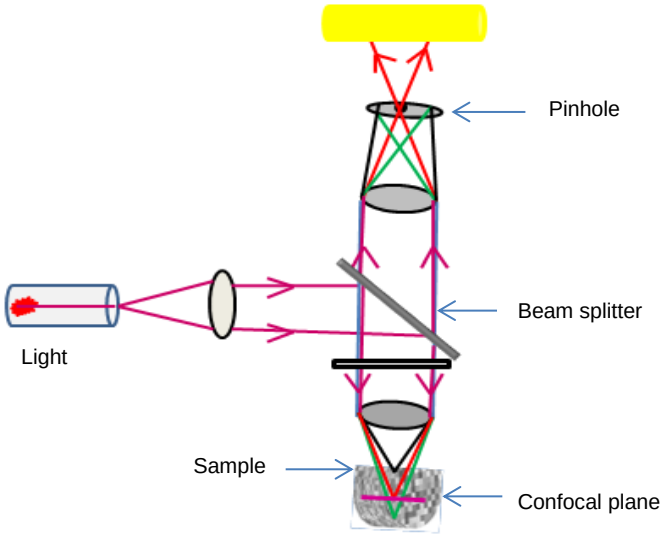

Fig. 2.3. Schematic diagram of the principle of confocal microscopy.

The components alignment, with a well-positioned pinhole to access only for those radiations reflected form confocal plane is as shown in Fig. 2.3. It consists of light source, scanners, the objective lens, intermediate lens, pinhole and detector. Narrow beams of light rays coming from the pointed laser source are allowed to fall on specimen and reflected rays were collected to image analyzer, charged coupled device CCD via pinhole (*0.25-1*AU), which only allows those reflected rays coming from the confocal planes and block reflections, which are off from the confocal plane. In the Fig. 2.3. green and black rays represent light reflecting from the points not in focal plane and red rays

are reflecting from the confocal plane. Well positioned pinhole allows only rays reflected form confocal plane (i.e. red color rays in the schematic picture) and eliminates other reflections (green and black). Ability to reduce out of focus blur and non-invasive optical sectioning with improved resolution makes confocal microscopy well suited for cytological study.

Well-aligned aperture system and x-y scanner in confocal microscopy helps us to gain high axial and lateral resolutions. For simple florescence microscopy, optical resolution is $r = 0.61\lambda / NA$, where, λ is the florescence wavelength of emission light and $NA = n * \sin\theta$ is numerical aperture that characterizes the range of angles over which the system can accept or emit light. In confocal microscopy, $r\_lateral = 0.37 / NA$ to $0.51\lambda / NA$ for pinhole size is 0.25 to 1 AU it is standard for all confocal microscopes and $r\_axial = 1.4\lambda n / NA$ [62].

Sample preparation and confocal calibration

Equal numbers of each type of cultured cells were plated in four wall chamber slides and allowed to attach approximately twenty four hour and processed for confocal microscopy, which includes rinsing, washing blocking and incubation (in Alexa Fluor® 488 secondary antibody). The cells are then dyed with DAPI to stain the nucleus. DAPI stained cells were mounted in cover slips with mounting medium FluoroCare Anti-Fade (BioCare Medical). Finally, confocal microscopy imaging was performed with an Olympus Fluoview FV1000 confocal microscope (Olympus Corporation) at magnification 600x. We have taken nearly hundreds of images from each type of cell lines AsPC-1, BxPC-3, HPAFPLKO, HPAF-Sh MUC13, Panc-1EGFP, Panc-1 MUC13 and recorded.

2.3 Construction of Refractive Index Matrix

Several studies have been done, and results of these studies they show a strong correlation between the nuclear optical refractive index and local mass-density in cell [63]. The changes in refractive index alteration have shown to be proportional to the local density of nuclear macromolecules such as double-stranded DNAs, RNAs, aggregated chromatin and bound proteins. ie. $n=n_o + \Delta n = n_o + \alpha\rho$, where, n_o is the refractive index of the medium surrounding a scattering structure, ρ is local concentration of solids and α is proportionality constant (specific refraction increment); its value is approximately 0.185 for majority of biological molecules found in living cells [64].

2.3.1 Refractive index matrix from TEM data

When highly accelerated electrons are focused on sample medium, they can scatter elastically or in-elastically and produce many signals such as auger electrons, secondary electrons, x-rays, light and other radiations as shown in Fig. 2.4. In principle, all these products of primary beam interaction between probing electrons and atoms of the sample medium can be used to derive information on the nature of the specimen. The selection of signal depends on working principle of microscopy technique. In TEM, only those electrons transmitted through the specimen are collected. These transmitted electrons are rich with bulk and surface information of specimen.

The intensity of electron beams transmitted through a spatial position *(x,y)* consisting of a voxel (volume = *dxdydz*) depends on the localized biomass in the voxel. If the bio mass present within a voxel is dense, TEM intensity will be less and if the corresponding biomass is rarer, TEM intensity will be more. Fig .2.5. shows the dependence of TEM intensity with atomic density and hence charge density of respective

voxel mass. Mathematically, TEM intensity is $I_{TEM} = I_o \exp(-\beta M(x,y))$, *M(x,y)* is biomass present on respective voxel, I_0 is the incident intensity, β is a constant which depends on characteristics of specimen (absorption and scattering coefficients) [65]. For very thin sample, its thickness is negligible compared to length and breadth. Therefore, for small value of M, $\exp(-\beta M) \approx 1 - \beta M$,we then obtain a linear relation between biomass present on respective voxel *M(x,y)* and TEM intensity i.e. I_{TEM} *(x,y)* α *M(x,y)*.

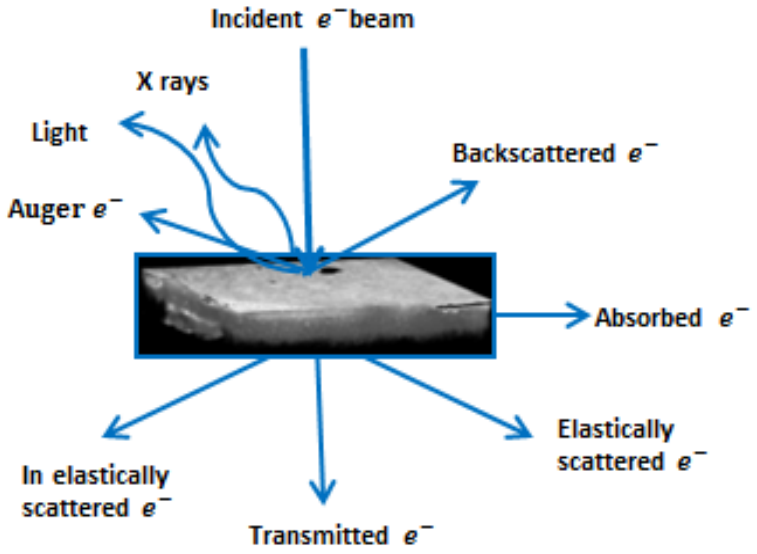

Fig.2.4. Different signals emitted due to interaction between incident electrons and atoms of sample medium.

By considering, mean background intensity I_o and fluctuating part of the intensity around the spatial point (x, y) of the pixel is $\Delta I(x, y)$, localized intensity of optical lattice at the respective pixel position *(x, y)* can be written as;

$$I(x,y) = I_o + \Delta I(x,y) \qquad \ldots\ldots (2.6)$$

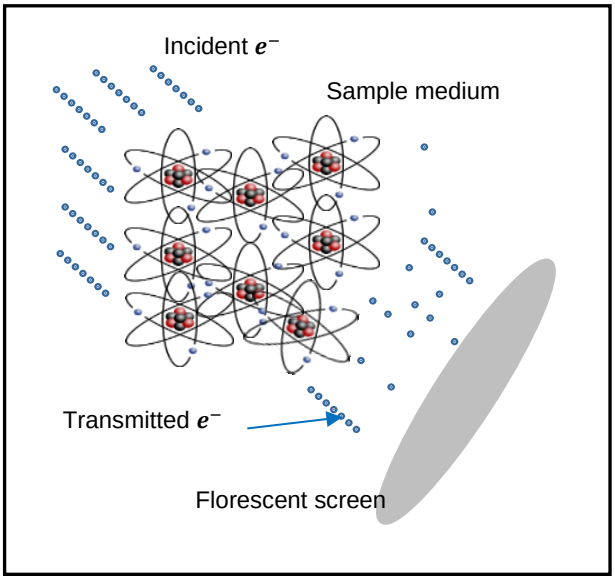

Fig. 2.5.Schematic diagram to show dependence of TEM intensity with biomass density and hence electron charge density present on the respective voxel.

Similarly, form the refractive index relation mentioned above, $n = n_o + \alpha\rho$, refractive index at the localized point *(x,y), n(x, y)* depends on biomass present within that voxel. For an ultrathin biological sample, we consider that the absorption of the contrast agent by the cell is linearly proportional to the total mass present in the thin cell voxel $n(x,y)\ \alpha\ M(x,y)$ and that the lattice is an effective optical lattice [16]. In terms of constant background refractive index of full sample n_o and fluctuating part $\Delta n(x, y)$, the refractive index at the voxel around the spatial point *(x,y), n(x,y)* becomes;

$$n(x,y) = n_0 + \Delta n(x,y) \qquad \ldots\ldots. (2.7)$$

$$n_{Effective} = n_{\mathrm{Re}al} + in_{\mathrm{Im}aginary} \qquad \ldots\ldots. (2.8)$$

Relations as given in equations (2.6) and (2.7) are true for all cells like dielectric optical media. The imaginary term of refractive index $n_{Imaginary}$ in equation (2.8), which characterizes the fluctuation in absorption (ionic behavior) is comparatively negligible for cells. Furthermore, the values of fluctuations part in refractive index $\Delta n(x, y)$ and intensity $\Delta I_{TEM}(x, y)$ are also comparatively small relative to their respective average values n_o and I_o ie. $\Delta n(x, y) << n_o$ and $\Delta I_{TEM}(x, y) << I_o$. Consequently, it can be shown that the effective (average) optical potential of ith optical lattice, ε_i for the voxel around the point *(x, y)* can be written as:

$$\varepsilon_i \alpha \frac{\Delta n(x, y)}{n_0} = \frac{\Delta I_{TEM}}{I_0} \qquad \ldots\ldots (2.9)$$

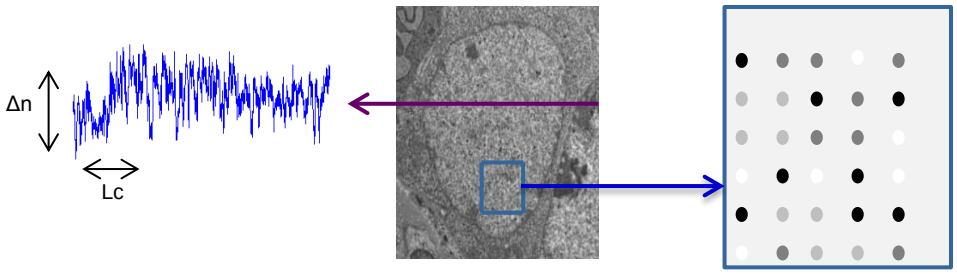

Fig. 2.6. Disordered optical lattice system constructed from TEM data.

Optical lattice systems (refractive index matrix) derived from TEM data are as shown in Fig.2.6. Grey scale dots with different intensity on the lattice site (right arrow) are numeric values of the localized refractive indices. The crest and trough of the wave (left arrow) with different amplitudes represents an axial fluctuation in refractive indices Δn with certain spatial correlation length (L_c).

2.3.2 Refractive index matrix from confocal data

Confocal microscopies of biological cells are performed in conjecture with florescent samples. For this reason, it is imperative to have a basic knowledge of florescence theory and imaging for confocal microscopy. Basic mechanism of florescence is as shown in Fig.2.7. The horizontal lines represent the quantum energy levels of the florescent dye molecule. When a high energy photon incident on the dye molecule at the lower energy state indicated by S_o, molecule raised to an excited energy state (S_1 or S_2 in the diagram) followed by losing little energy to other molecules and drops to lower excited state. The emission spectrum is typically a mirror image of the S_o to S_1 absorption spectrum transition.

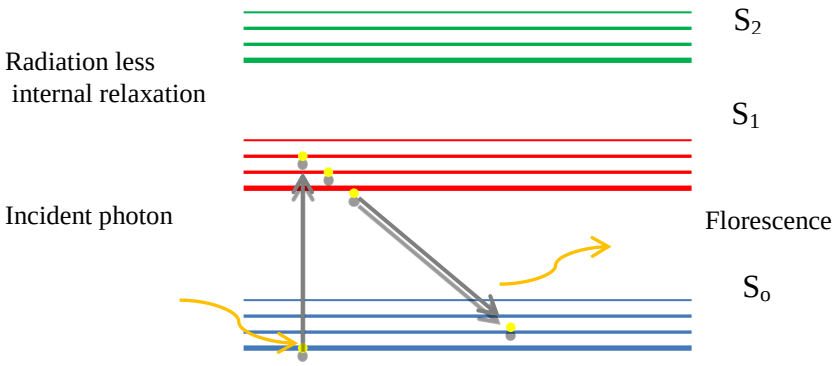

Fig. 2.7. Jablonksi diagram of excitation and florescence.

To understand the interaction between signal and sample, it has been shown that the rate of absorption of photons when the light is incident on the sample medium is $k_a = \sigma I_i$ where σ cross sectional area and I_i is the illumination intensity. Saturation occurs when the rate of absorption is equal to decay rate of excited state, which is given by $k_e = \sigma I_s$, where I_s is the saturation intensity. For the confocal imaging under

saturation condition, it is assumed that florescence intensity is linear function of the illumination intensity $I_{fl} \propto I_i$ and $I_i \ll I_s$. Furthermore, the laser beam has a Gaussian cross-section in intensity and is specified by its waist parameter w and power points in a localized position $\vec{r}$ = *(x, y, z)*, as given by equation (2.10) [66].

$$I(\vec{r}) = I_o e^{-2\vec{r}^2 / w^2} \qquad \text{……. (2.10)}$$

In the following, we will derive the relationship between the voxel and the probing intensity for confocal images. For the probe with center r_c = *(x_c, y_c, z_c)*, the illumination intensity at any point $\vec{r}$ = *(x, y, z)* is given by;

$$I_i(\vec{r}, r_c) \approx \exp\left[-2\left(\frac{(x - x_c)^2 + (y - y_c)^2}{W_{xy}} \right) - 2\left(\frac{(y - y_c)^2}{W_z} \right) \right] \qquad \text{……. (2.11)}$$

where, w_{xy} is lateral and w_z is axial width of the beam. Therefore, the detection probability distribution for an arbitrary illumination volume V_i is given as;

$$P_i(\vec{r}, r_c) = \frac{I_i(\vec{r}, r_c)}{I(\vec{r}, r_c)} \qquad \text{……. (2.12)}$$

Furthermore, in typical florescence experiment, the intensity required to excite a volume is directly proportional to the mass density inside that volume and the detection intensity proportional to probability multiplied by illumination intensity.

$$I_{\det}(\vec{r}, r_c) \sim P(\vec{r}, r_c) * I_i(\vec{r}, r_c)$$

$$I_{\det}(\vec{r}, r_c) \sim [I_i(\vec{r}, r_c)]^2 \qquad \text{……. (2.13)}$$

Therefore, if we construct an optical grid system by point-to-point mapping from confocal micrographs, the optical potential for i^{th} lattice/matrix site is as given in equation 2.14. Fig 2.8. shows the construction of optical refractive index array/ matrix system from the confocal micrograph. A point-to-point mapping is done from the confocal micrograph to construct same size optical lattice system representing the refractive index values inside the corresponding pixels.

$$\varepsilon_i \alpha \frac{\Delta n(x, y)}{n_o} \alpha I_i \alpha (I)^{1/2} \qquad \text{…….(2.14)}$$

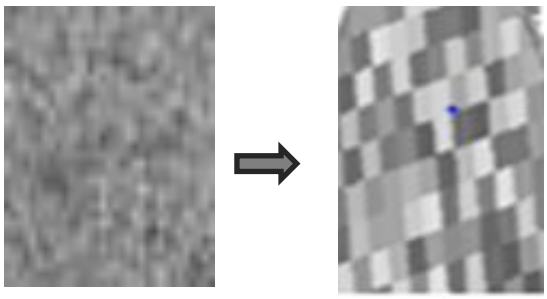

Fig. 2.8. Construction of disordered optical lattice/ matrix system by point-to-point mapping from confocal microscopy image.

2.4 Tight Binding Hamiltonian

Anderson's disordered tight binding model (TBM) has been well studied in condensed matter physics to analyze disorder in a lattice system [67,68]. It has been proven a good model for describing localized optical states of systems of any geometry and disorder. Therefore, we have solved the Maxwell equations for the aforementioned

disordered lattice/matrix sample in closed boundary condition, which gives the eigenvalues and eigenfunctions. Light localization property of the disorder optical lattice system is than analyzed by calculating the inverse participation ratio (*IPR*) of the eigenfunction of the system as described in the following section.

By considering one optical state of photon per lattice site, and the inter lattice site hopping are restricted to the nearest neighbors only. A tight binding Hamiltonian with |i> and |j> optical wave functions for respective i^{th} and j^{th} lattice sites with overlap integral t, i^{th} lattice optical potential or refractive index energy (eigenvalue)ε_i is

$$H = \sum_i \varepsilon_i |i\rangle\langle i| + t\sum_{\langle ij\rangle} (|i\rangle\langle j| + |j\rangle\langle i|) \quad \text{……. (2.15)}$$

2.5 Inverse Participation Ratio Analysis to Quantify Structural Disorder

The quantum mechanical concept of inverse participation ratio (IPR) has been well studied in different branches of physics for disorder quantification. It gives the quantitative measurement of atoms delocalized over a bond, even when the probability distribution is not uniform. Along with the development of nanotechnology, this concept has been extensively reviewed and generalized to different applications in Condensed Matter Physics [69]. Implication of *IPR* technique for biological media is also validated in references [16,37].

Technically, the IPR of a fluctuating wavefucntion $\psi(\vec{r})$ in D-dimensions is defined as

$$IPR = \int d\vec{r} \left|\psi(\vec{r})\right|^{2D} \quad \text{……. (2.16)}$$

In units of inverse area in two dimensions;

$$IPR = \int d\vec{r} \left| \psi(\vec{r}) \right|^4 \qquad \text{……. (2.17)}$$

More generalized form of average *IPR* over all of the N eigenfunctions of IPR pixels (i.e. $<IPR>_{Pixel}$) in a system in an optical 2D lattice (IPR pixels) *LxL* is

$$\left\langle IPR(L) \right\rangle_{Pixel} = \frac{1}{N} \sum_{i=1}^{N} \int_0^L \int_0^L E_i^4(x, y) dx dy \qquad \text{……. (2.18)}$$

where, E_i is the i^{th}, eigenfunction of the Hamiltonian of optical lattice of size *LxL*, dx = dy = a are the length scale of each pixels. Total number of Eigenfunctions *N*, number of lattices along each axis of *2D* plane (L_a), lattice size *LxL* and are of each pixels are related as; $N = L_a^{\,2} = (L/a)^2$.

Average IPR at specific length scale, of a uniform lattice is a fixed universal number and it increases with increase in degree of disorder (or degree of localization) [37]. Proportionality relation between *IPR* and disorder strength can be written in terms of refractive index fluctuation $(\Delta n)$and corresponding correlation decay length (l_c) as;

$$IPR \quad \alpha \quad L_d = \Delta n^2 x l_c \qquad \text{..... (2.19)}$$

CHAPTER 3

RESULTS AND DISCUSSION

A majority of diseases are the cause of disturbances at the cellular level, so the cytology becomes increasingly important for the early detection of the disease level. Cancer, a deadly malignant collection of diseases, and alcoholism, a disease inducing practice, are associated with the alteration in genetic performance. Therefore, we have focused our study in the nuclear region of effected tissues, which is a critical organelle where genes are located. Our analyses include the statistical analysis and quantification of the degree of structural disorder in nucleus to obtain the average and STD of structural disorder or statistical IPR values. Nano to submicron scales of morphological alteration of nuclear components reflected as the spatial mass-density fluctuation due to carcinogenesis and/or alcoholism in different bodily sites were studied by using conventional microscopies. Depending on the use of microscopy types and sample studies, the result of this work is divided into following sections.

3.1 Results of TEM Studies

We have used the transmission electron microscopy (TEM) for the detection of the aggravation effect of alcoholism in early colon cancer and hippocampal morphology in adult (10-12 weeks) female C57BL6 mice. Aforementioned, electron transparent and mechanically robust samples derived from colonic and hippocampal biopsies of each type of mice models were imaged in the identical conditions and were analyzed. First we have taken fifteen (3 mice per group, 5 micrographs/mice, total 15 micrographs) TEM micrographs from every type. Studied mice models involve (i) normal (Control), (ii) alcoholic (Control treated with EA), (iii) early colon carcinogenesis (AOM/DSS) (iv)

alcoholic mice with early colon carcinogenesis (DSS/AOM treated with EA) for colon cancer. Similarly, in second project, alcoholism and neurological disorder project, we have taken fifteen (3 mice per group, 5 micrographs/mice, total 15 micrographs) TEM micrographs from the nuclear region of hippocampus from each samples (i) normal (Control) and (ii) Alcoholic (Control + EA).

3.1.1 Alcoholism and progression of colon cancer

To study the role of alcoholism for the initiation and progression of colon carcinogenesis, TEM images of colon cell nucleus of (i) normal (Control) mice (ii) alcoholic mice (Control+EA) (iii) early carcinogenic mice (AOM+DSS), and (iv) early carcinogenic alcoholic mice (AOM+DSS+EA) have been analyzed. Respective grey scale images, corresponding IPR images and quantified average IPR values from each type were compared.

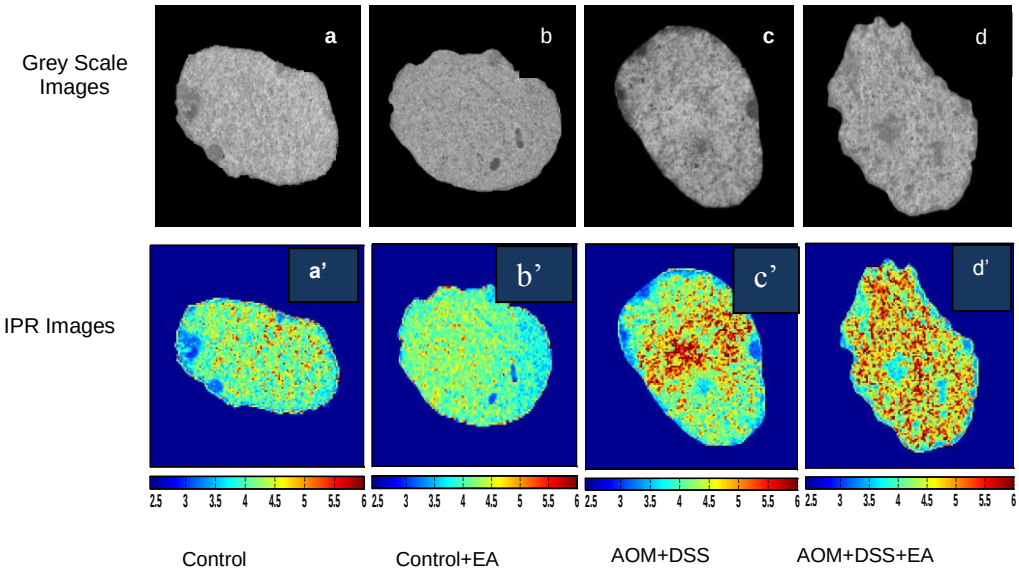

Fig.3.1. Rrepresentatives of TEM grey scale images and corresponding IPR images (IPR pixel size LxL = 50nm x 50 nm) of colon cell nucleus derived from normal, alcoholic, early colon cancerous and alcoholic early colon cancerous mice.

Fig. 3.1. (a), (b), (c) and (d) are the representative TEM grayscale micrographs of colon cell nucleus of normal mice, alcoholic mice, early colon carcinogenic mice and early carcinogenic plus alcoholic mice respectively. Only a comparative study of greyscale intensity TEM images of intracellular mass taken from respective untreated/treated mice groups does not guarantee the morphological difference for visual inspection. We then compared the respective IPR images, derived from each type of TEM grayscale images, which show the difference in disorder fluctuation clearly. Fig. 3.1 (a'), (b'), (c') and (d') show the corresponding IPR images (IPR pixel dimension 50 nm x 50 nm).In the IPR images, the spatial fluctuation in each color patterns which represents refractive index fluctuation, increases as we go from a' to c' and c' to d' but identical between a' and b'. Fluctuation in localized color patterns on IPR pixels has direct correlation with refractive index fluctuation of medium and hence with the nanoscale mass density fluctuation. Redness in the IPR images shows the more disorder and blueness in the IPR represents less disorder.

TABLE 3.1

QUANTIFIED VALUES OF < IPR> FOR DIFFERENT SAMPLE LENGTH OF COLON CELL NUCLEI WITH DIFFERENT MALIGNANCY

Sample L (nm)	Control	Control+EA	AOM+DSS	AOM+DSS+EA
12.5	2.25	2.28	2.35	2.38
25	2.96	2.99	3.17	3.24
37.5	3.47	3.50	3.78	3.89
50	3.92	3.95	4.34	4.50
62.5	4.34	4.38	4.90	5.11
75	4.76	4.81	5.48	5.73

Localized fluctuation in refractive indices represented as IPR images were further quantified at different length scales of sample length (IPR pixel values). These quantified values of average IPR pixel for sample length values 12.5 nm, 25 nm, 37.5 nm, 50 nm, 62.5 nm and 75 nm are as shown in Table 3.1. Fig.3.2.A shows the graphical representation of $<<IPR(L)>_{Pixel}>$for different values of sample length (L) 12.5 nm to 75 nm(averaged over n = 15). The length scale dependent average of $<<IPR(L)>_{Pixel}>$ for each disorder sample increases with the sample size and disorder concentration. The decreasing slope of graph further suggests to us that the rate of fluctuation is going to saturate for the higher value of length scale and it will give a uniform value like a uniform sample. Most importantly, the results show that alcoholism has less effect for colon cancer initiation but it plays an important role for the colon cancer progression because the result shows average IPR values that are almost identical for normal and alcoholic cases, but there is a significant difference between early carcinogenic and early carcinogenic with alcoholism.

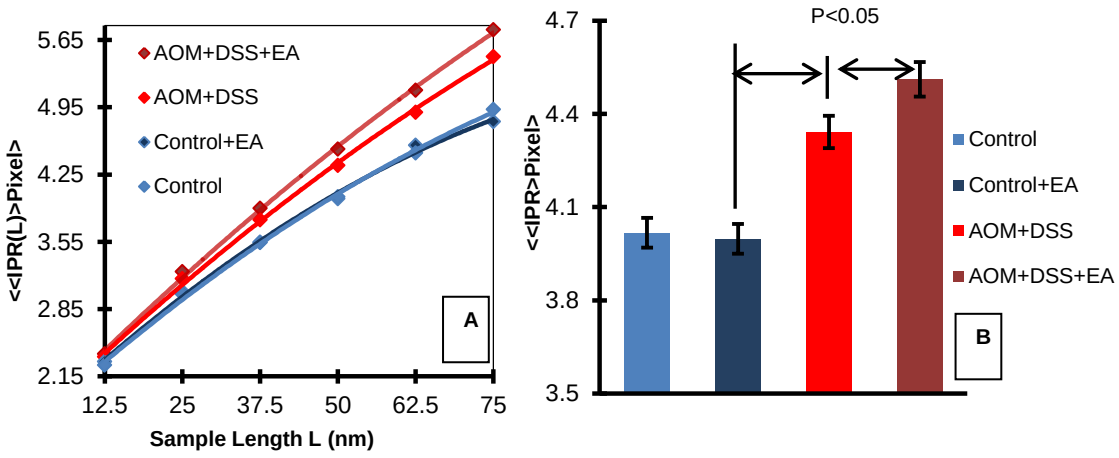

Fig. 3.2. A. Ensemble-averaged (n=15) values of $<<IPR(L)>_{Pixel}>$ versus L (in nm) plots,B.Histogram of $<<IPR>_{Pixel}>$forpixel size LxL = 50nm x 50nm, for nucleus of colon cells.

The length scale dependent analysis of $\langle IPR \rangle_{Pixel}$ at sample length LxL = 50nm x 50nm are also represented into histogram as shown in Fig. 3.2.B. At this length scale, the average IPR values are nearly same for normal and alcoholic ($4.02 \approx 3.99$) but there is significant difference between normal and early carcinogenic ($4.02 < 4.34$), and early carcinogenic ($4.34 < 4.51$). Student's t-test two-tailed unequal variance p-value is also statistically significant for each case. Its value is less than 0.05 while comparing AOM/DSS and AOM/DSS with EA and is more than 0.05 while comparing Control and Control plus EA. Similar trend can be seen in other length scales too.

TABLE 3.2

QUANTIFIED VALUES OF < IPR > FOR DIFFERENT SAMPLE LENGTH OF COLON CELL'S PERI NUCLEAR REGION WITH DIFFERENT MALIGNANCY

Sample L (nm)	Control	Control+EA	AOM+DSS	AOM+DSS+EA
12.5	2.24	2.27	2.32	2.34
25.0	2.95	2.98	3.11	3.14
37.5	3.42	3.43	3.64	3.69
50.0	3.80	3.79	4.07	4.16
62.5	4.11	4.10	4.43	4.58

In addition to the whole nucleus, perinuclear regions were also probed for this study because this region provides the pathway for transportation and interacts first with injected/ingested drugs or chemicals before the core and morphological alteration inside nucleus has strong correlation with interface area. Result follows the similar trend as the whole nucleus, but average IPR values are slightly less than in previous case (whole nucleus) for all the length scales.

The average IPR values for sample length 12.5nm, 25nm, 37.5nm, 50nm and 62.5 nm are shown in table 4.2. Fig.3.3 is the graphical representation between $<<IPR>_{pixel}>$ versus sample length L (in nm) for the perinuclear region of differently treated colon cell nucleus. Which clearly shows average IPR and hence nanoscale spatial mass density fluctuation is higher for cancerous compared to noncancerous and early cancerous administered with-ethanol compared with without-ethanol and similar for normal and alcoholic for all the length scales measured. Bar graph representation for mean IPR values for length scale 50 nm verifies the statistical significance of our comparative analysis.

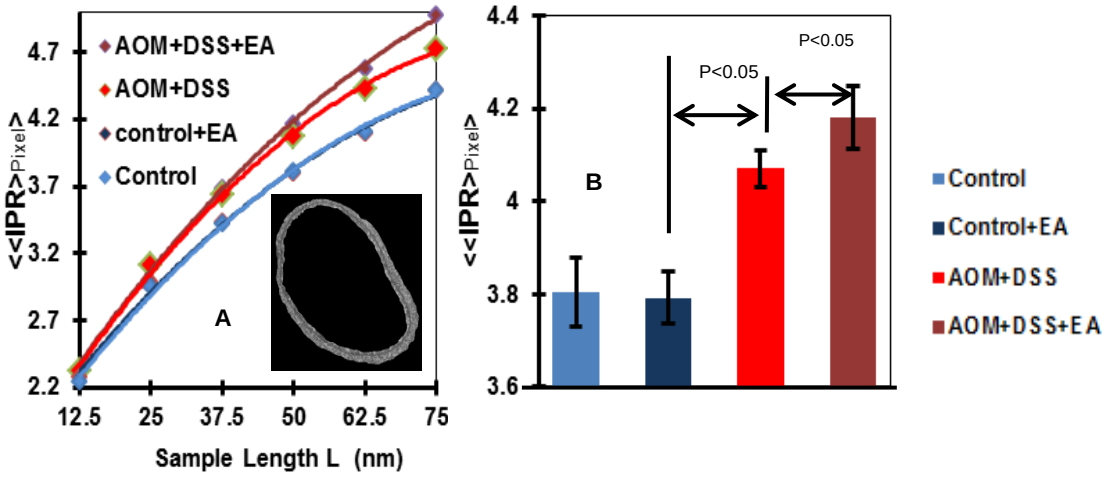

Fig. 3.3. A. Ensemble-averaged (n=15) values of$<<IPR(L)>_{Pixel}>$ versus L (in nm) plots, B. Histogram of <<IPR>Pixel>for pixel size LxL = 50nm x 50nm, for perinuclear region of colon cells.

3.1.2 Alcoholism and neurological disorder

Hippocampal cellular nuclei subjected with alcohol have more disorder than their healthy counterparts. Fig. 3.4. (a) and 3.4. (b) are the representative of TEM grayscale micrographs obtained from hippocampal cellular nucleus of normal (Control) mice and

alcoholic (Control+EA) mice respectively. Corresponding IPR images in two dimensions (IPR pixel dimension 130 nm x 130 nm) are as shown in Fig. 3.4.a' and b' respectively. The IPR images of these TEM micrographs, matrix representations of the degree of structural disorder created form respective images, and this clearly indicates the difference in disorder for cell nucleus for control and alcohol treated. The intensity representation of IPR matrices are shown in a'' and b''. It can be shown in the graph that higher variation in IPR or structural disorder intensity for alcoholic mice.

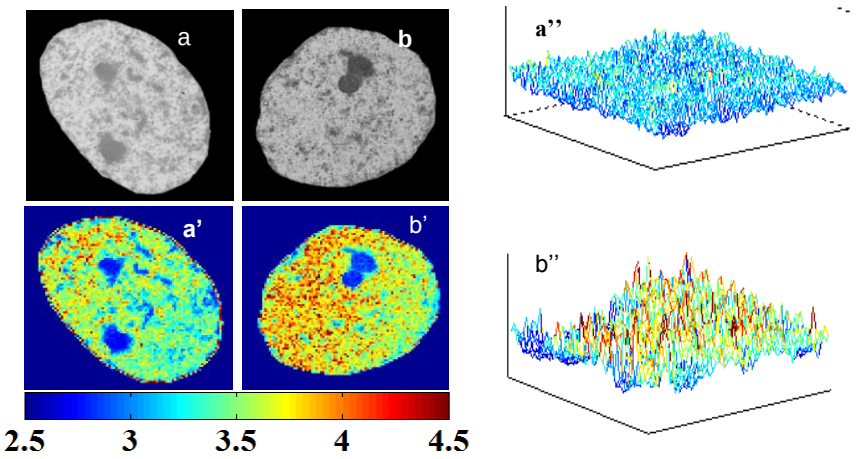

Fig. 3.4. (a) and (b) are rrepresentative of TEM grey scale intensity, (a') and (b') corresponding 2D color IPR (130nm x 130nm) and (a'') and (b") IPR intensity images of hippocampal nucleus from normal and alcoholic mice.

Length scale dependent quantified values of disorder, i.e., the average <IPR> values, are expressed in the form of mean and standard deviation, and are shown in table 4.3. Mean and standard deviation of IPR are then plotted graphically for different sample length values 32.5nm, 65nm, 97.5nm, 130nm, 162.5nm, and 195nm. The average IPR pixel i.e. $\langle\langle IPR(L)\rangle_{Pixel}\rangle$ and standard deviation of IPR pixel ie. $\sigma(\langle IPR(L)\rangle_{Pixel})$ for two

different cases: (i) Hippocampal cell nuclei of normal mice and (ii) Hippocampal cell nuclei of mice with alcohol were graphically represented in Fig. 3.5. A and Fig. 3.6. A. These figures show that both average IPR and STD of IPR are more for chronic alcoholic mice and less for control (normal) mice for all sample length scale *L*. In the first graph, average value of mean IPR increases with decreasing slope along with sample size but in second graph the average value of STD of IPR increases with increasing slope along with sample size.

TABLE 3.3

QUANTIFIED VALUES OF <IPR> AND σ(IPR) FOR DIFFERENT SAMPLE LENGTH OF HIPPOCAMPAL CELL NUCLEI

Sample L (nm)	Average of mean (IPR)		Average of Standard Deviation IPR	
	Control	ControlEA	Control	ControlEA
32.5	2.17	2.20	0.132	0.136
65	2.77	2.86	0.207	0.232
97.5	3.16	3.31	0.274	0.297
130	3.48	3.69	0.343	0.366
162.5	3.77	4.06	0.426	0.452
195.00	4.05	4.43	0.480	0.562

The significance of statistical data was tested by mean bar graph histogram representation of both average values mean IPR and standard deviation of IPR as shown in Fig. 3.5 B and Fig. 3.6. B. Student's t-test two-tailed unequal variance p-value is 0.0015 for the case of ($<<IPR(L)>_{Pixel}>$) and 0.0237 in the case of $\sigma(<IPR(L)>_{Pixel}$ in the case of sample length 195 nm. In each case, the p value is less than 0.05.

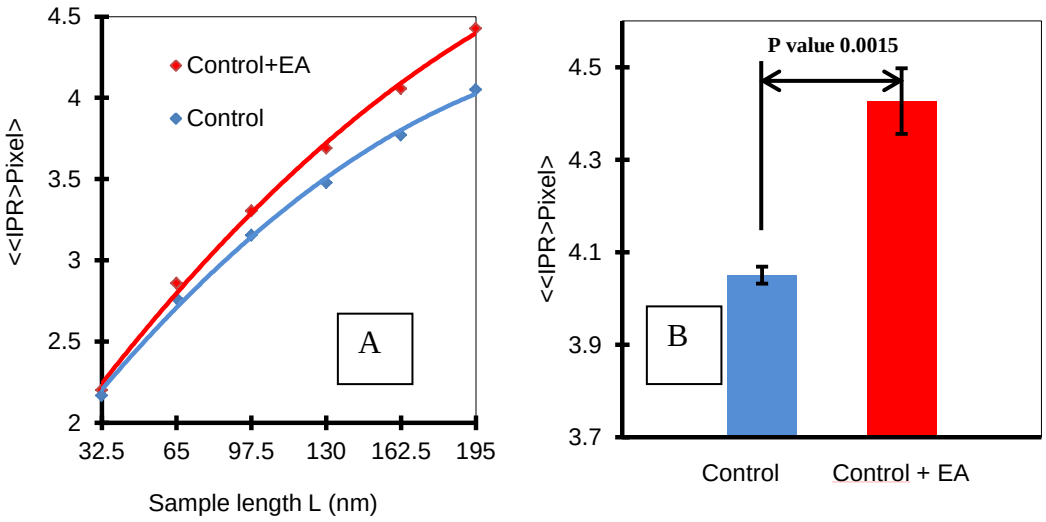

Fig. 3.5. A. Ensemble-averaged (n=15, 3 mice/group and 5 image/mice) values of<<IPR(L)>$_{Pixel}$> versus L (in nm) plots, B. Histogram of <<IPR>$_{Pixel}$> for pixel size LxL = 50nm x 50nm, for nucleus of hippocampal cells.

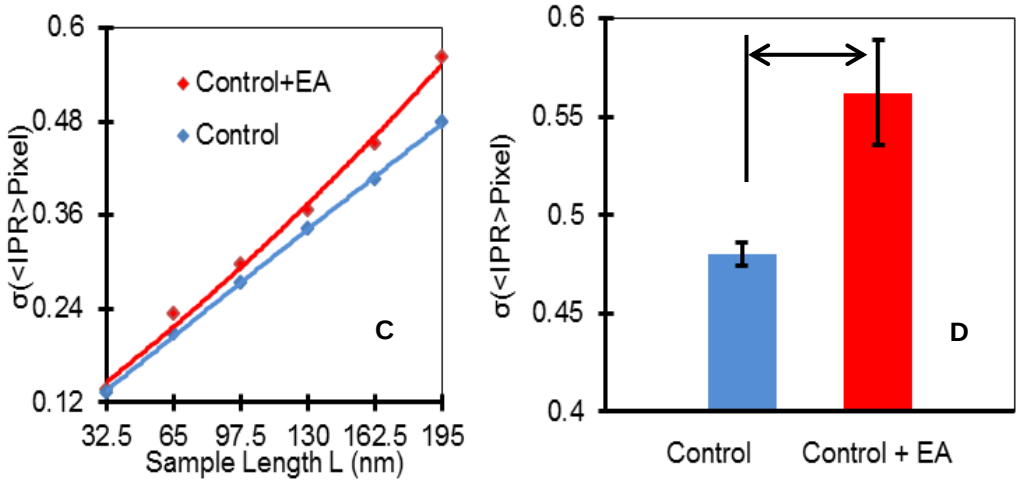

Fig. 3.6. C. Ensemble-averaged (n=15) values of σ<IPR(L)>$_{Pixel}$ versus L (in nm) plots D. Histogram representation at σ <IPR>$_{Pixel}$ for pixel size LxL = 195nm x 195nm, for nucleus of hippocampal cells.

3.2 Result of Confocal Studies

In our confocal study, we have used MUC13 protein expressions as the potential biomarker to study the aggravation stage of pancreatic cancer. Our results show the existence of proportional relation between MUC13 mucin expression and the stage of pancreatic cancer. This novel approach is used to analyze the nuclear morphological changes in different level of pancreatic cancer cell lines considered here AsPC-1, BxPC-3, Panc-1 EGFP, Panc-1 MUC13, HPAF PLKO and HPAF –sh MUC13. We have done the comparative study between (i) AsPC-1and BxPC-3, (ii) Panc-1 EGFP and Panc-1 MUC13, and (iii) HPAF PLKO and HPAF –sh MUC13.

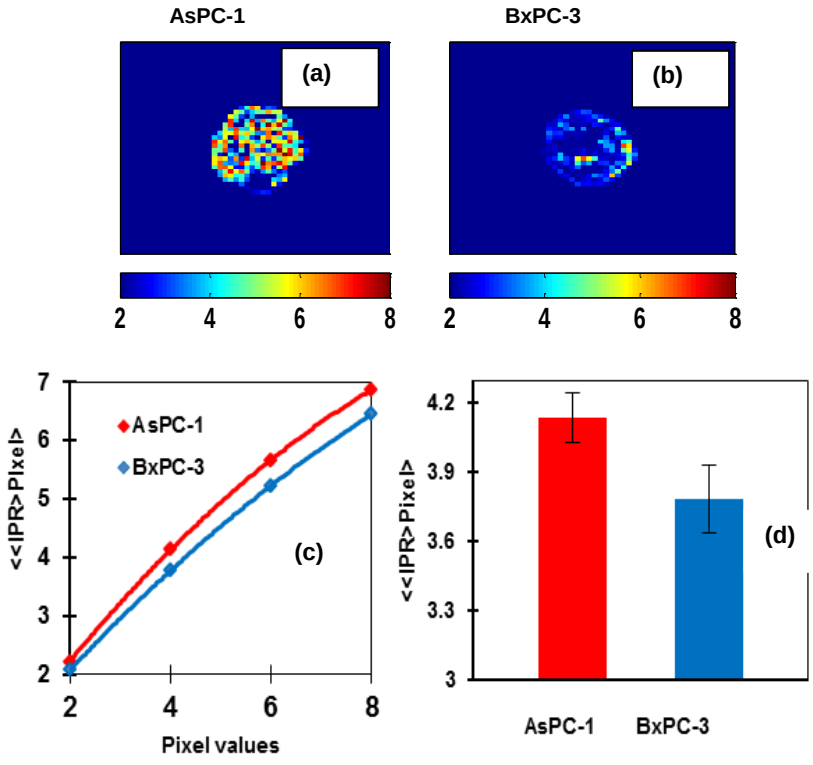

Fig.3.7. Comparative study between AsPC-1 and BxPC-3 cell lines. (Averaged over n=15)

First, we have compared the submicron scales of disorder fluctuations in human pancreatic carcinoma by analyzing the submicron scales of disorder in AsPC-1and BxPC-3 cancer cell lines. In AsPC-1 (trans-membrane mucin MUC13 are expressed) cancer cell lines, adeno-carcinoma is on the head of pancreas, metastases to the several abdominal organs. Similarly, in BxPC-3 adeno-carcinoma is on the body of pancreas and no evidence of metastasis or MUC13 expression. Fig. 3.7. (a), (b) show the IPR images of AsPC-1, IPR images of BxPC-3 cancer cell lines, (c) sample size dependent variation of average IPR for different values of pixel size (m=2,4,6 and 8 pixels), and (d) bar graph representation of average IPR for a constant sample size m=4. These graphs clearly show that the submicron scale of morphological alteration of nuclear components is more in MUC13 protein expressed pancreatic cancerous cell lines AsPC-1 compared to MUC13.

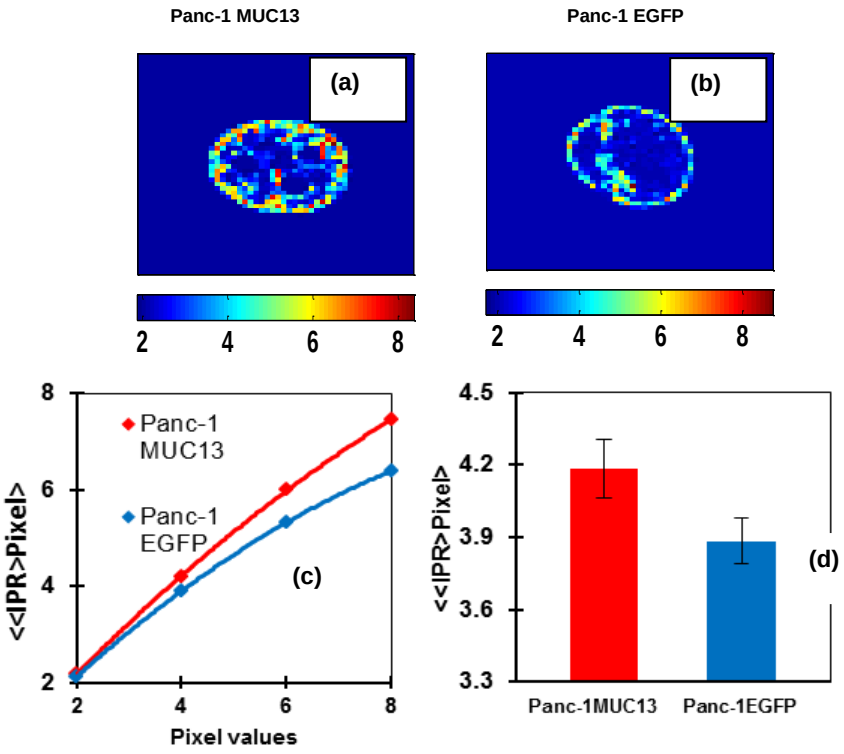

Fig.3.8. Comparative study betweenPanc-1 EGFP and Panc_MUC13 cell lines. (Averaged over n=15)

For a better understanding of the association between MUC13 mucin expression in pancreatic cancer and morphological alteration of intracellular mass, we have further analyzed the submicron scales of mass density fluctuation in Panc-1 MUC13 and Panc-1 EGFP pancreatic cancer cell lines. Where, Panc-1 EGFP does not have naturally expressed MUC13 mucin and MUC13 mucin is artificially induced in Panc-1 EGFP form chemical therapies and it is called Panc-1 MUC13. Fig. 3.8 shows the representatives of IPR images and graphical representation of quantified values of IPR for different sample length values. Result shows sub-micronscale structural fluctuation is is more for Panc-1 MUC13 types compared to Panc-1 EGFP for all the length scales measured.

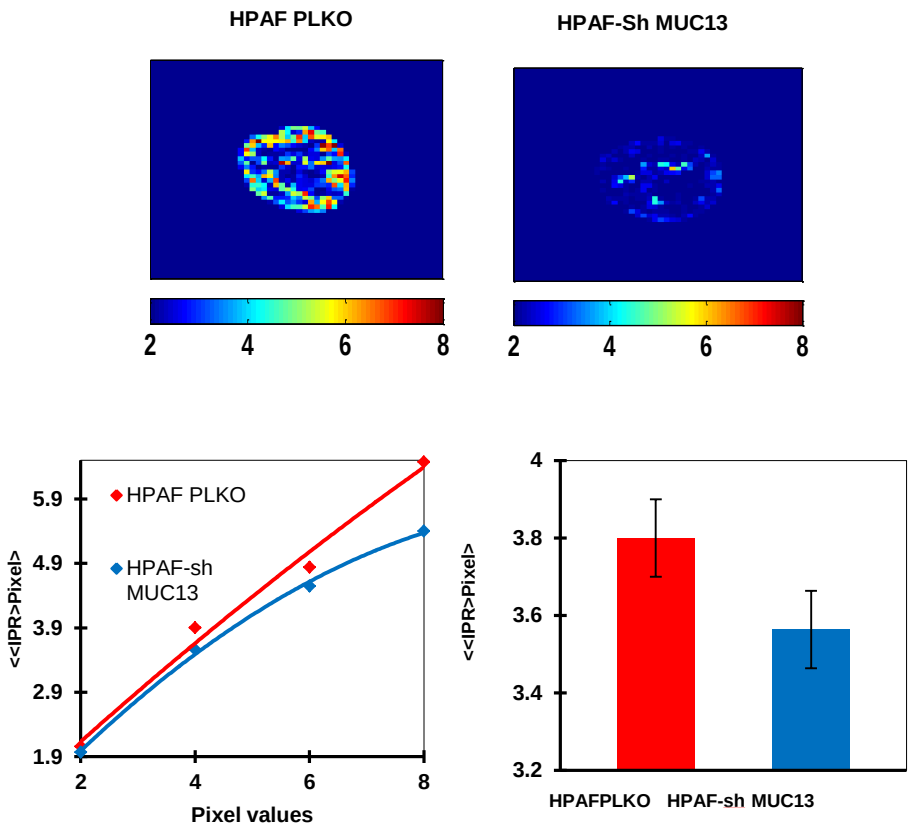

Fig. 3.9. Comparative study between HPAF PLKO and HPAF sh MUC13 cell lines. (Averaged over n=15)

Furthermore, we have extended our study to the HPAF PLKO and HPAF-sh MUC13 pancreatic cancer cell lines. Here, the HPAF PLKO cell lines have naturally available MUC13 expression, and we have knocked down the expressed MUC13 mucin by removing these expressed protein using chemical treatments to get HPAF-shMUC13, which does not have MUC13 expression. Submicron scales of morphological alterations were quantified and different pixel values as shown in Fig. 3.9. It can be seen from the figure that average IPR value is more for all the measured pixel size (number of pixels) for HPAF PLKO compared with HPAF-sh MUC13.

CHAPTER 4

CONCLUSION AND FUTURE WORK

The analyses of intracellular nanoscale as well as sub-micron scale morphological characteristics have shown significant promise to quantify levels of malignancy before the changes become pathologically evident. We have investigated the nuclear morphological alteration reflected as nano to sub-micron scales spatial fluctuation in nuclear mass density of normal cell and diseased cells (cancerous and alcoholic) at different level of malignancy. Our findings show a proportional relation between disease level and degree of intra-nuclear mass density fluctuations. Our study technique is unique, which first converts spatial fluctuations in mass density into spatial refractive index fluctuations, via TEM or confocal microscopy imaging, and then analyze these refractive index fluctuations by using the IPR technique a concept borrowed from Condensed Matter Physics. This unique technique enables us to quantify nanoscale of spatial fluctuation in intracellular heterogeneity in a single parameter, i.e., structural disorder $<IPR> \sim \Delta n * L_c$ (where, Δn is fluctuation in refractive index with correlation length l_c). On the basis of our results, conclusion section in the following is divided into two sections.: (i) Results from TEM studies, and (ii) results from confocal studies.

(i) Conclusion form TEM Studies

TEM study enables us to analyze nanoscale intracellular morphological alteration within the intranuclear mass density fluctuations. We have analyzed two malignant problems via TEM imaging, which are: (i) effect of alcoholism on colon cancer and (ii) effect of alcoholism on neurological disorder.

Conclusions from colon cancer studies

First, we report the effect of alcohol on normal and pre-cancerous colon intracellular mass by using nanoscale structural disorder as a biomarker for early cancer diagnosis. The effect of alcohol on normal and precancerous colon cells using AOM-mice model via TEM imaginghas shown promising results to quantify malignant level before these become microscopically evident for visual inspection. The quantified value of disorder parameter <IPR> ~Δn*Lc for nanoscale level points the following results:

(1) Alcohol does not have a significant effect related to carcinogenesis on normal colonic cells. The degree of structural disorder parameter, $L_{sd}=\Delta n^{2} * L_c$, has not changed significantly as we compare between normal and alcohol treated normal mice. For all the length scales measured, average values of IPR are equivalent between normal mice and alcohol treated mice.

(2) The colon cell nuclei show a significant increase in the nanoscale structural disorder in progressive carcinogenesis, relative to normal or pure alcohol treated normal cell nuclei. For every length scales measured, average IPR value of AOM-mice without alcohol treatment is significantly higher when compared to a normal one. In particular, the degree of structural disorder, Lsd, value increases with the progression of carcinogenesis.

(3) The colonic nuclei for alcoholic AOM-mice show higher values of structural disorder L_{sd} relative to the nonalcoholic AOM-mice cells nuclei. This result implies that alcohol is an enhancer to the carcinogenic progression, when some carcinogen was present. In particular, our results show that there is no visible effect of alcoholism on normal colon cells but alcohol administration enhances the early carcinogenic aggravation rate.

Conclusions from neurological studies

Another important finding from our study using TEM is the effect of alcoholism in neurological disorder by analyzing the nanoscale morphological alteration in the intracellular mass of the hippocampal region via transmission electron microscopy. This approach of analyzing the effect of alcohol in the brain region is more accurate than present available techniques, such as magnetic resonance imaging (MRI) and light microscopy (Golgi's method),for the dimensional analysis of hippocampal bulk mass, because it is also difficult to quantify the fractional contribution of alcoholism for the volumetric alteration. Other factors like age, lifestyle, thinking level etc. also contributes for the volumetric alteration. Therefore, this approach of nanoscale morphological analysis by using IPR technique could be the more accurate and sensitive technique that can precisely reflect the level of aggravation of carcinogenic processes in the hippocampal region. Results of our findings using nanoscale sensitive techniques IPR analysis of localized eigenfunctions derived from respective cellular nuclei show that the hippocampal cell nuclei of alcohol-administered mice have more spatial nanoscale structural disorder/fluctuation compared to those of normal mice.

(ii) Conclusion form Confocal Studies

Using confocal technique, we have studied the aggravation stages of pancreatic cancer at different level of MUC13, a transmembrane mucin involved in pancreatic cancer progression. The analysis of submicron scales of alteration in nuclear morphology shows submicron scale of spatial mass density fluctuation is more in the naturally MUC13 mucin expressed pancreatic cancer cell lines AsPC-1 (more aggressive form of pancreatic cancer) and less in non-expressed pancreatic cancer cell lines BxPC-3 (less

aggressive form of pancreatic cancer). There is proportional relation between miscron scale intracellular mass density fluctuation and MUC13, a transmembrane mucin involved in pancreatic cancer progression

Result of our extended work in this project, which involves the alteration in MUC13 mucin expression by therapeutic approach and analyzes morphological alteration, is more encouraging for oncological studies. Submicron scale of morphological alteration increases as we express the MUC13 mucin by chemical therapies in naturally MUC13 unexpressed cell lines. Panc-1 EGFP does not have expressed MUC13 mucin, and we therapeutically expressed protein and called Panc-1 MUC13. Similarly, the submicron scale morphological alteration decreases as we suppress the MUC13 mucin by chemical therapies in naturally MUC13 expressed cell lines. HPAF PLKO has naturally expressed MUC13 mucin, and we therapeutically suppress the protein called HPAF-shMUC13. Both of these studies show the level of mucin expression in the epithelial mass of the pancreas, which determines the aggressive level of cancer cells. We can therapeutically alter the cancer aggressive level by expressing or suppressing MUC13 mucin.

(iii) Future Scope

A majority of malignancies are not detectable and difficult to discern for several years. To have a growth that is visible to the present pathological microscopy, the cancerous mass must have begun developing many years ago. The genetic predispositions, environmental circumstances and personal behaviors enhance the rate of aggravation for malignancies. Therefore, it is important to detect earlier malignant conditions and avoid the adoption of cancer causing environment and behaviors. Our

study technique involves the quantification of nanoscale level of mass density fluctuations in the biological medium, by using a mesoscopic physics approach, which supports a better understanding of malignancy, if it is associated with structural rearrangement of intracellular mass density variation/fluctuations. Similar to our study in alcoholism, we can extend this technique for other diseases for cells such as cells are in drugs, and radiations.

Furthermore, currently, the rate of diagnosis exactly matches with the rate of death for pancreatic cancer. Our findings could be a potential technique for pancreatic cancer treatment by suppressing expressed MUC13 mucin and open door for more studies.

REFERENCES

[1] A.I. Lamond and W.C Earnshaw, "Structure and function in the nucleus," *Science*, vol. 280, no. 5363, pp. 547-553, 1998.

[2] T. Cremer and C. Cremer, "Chromosome territories, nuclear architecture and gene regulation in mammalian cells," *Nature reviews genetics*, vol. 2, no. 4, pp. 92-301, 2001.

[3] P.L. Yeagle, "Lipid regulation of cell membrane structure and function," *The FASEB journal*, vol. 3, no. 7, pp. 1833-1842, 1989.

[4] G. Karp, *Cell biology*.6th ed. John Wiley & Sons, New Jersey, 2010.

[5] S.P. Jackson and J. Bartek, "The DNA-damage response in human biology and disease," *Nature*, vol. 461, no. 7267. pp. 1071-1078, 2009.

[6] S. Chen, M. Zhao, G. Wu, C. Yao and J. Zhang, "Recent advances in morphological cell image analysis," *Computational and Mathematical Methods in Medicine*, 2012.

[7] S.W. Chan, K.S. Leung and W.F. Wong, "An expert system for the detection of cervical cancer cells using knowledge-based image analyzer," *Artificial Intelligence in Medicine*, vol. 8, no. 1, pp. 67-90, 1996.

[8] D. Glotsos, P. Spyridonos, D. Cavouras, P. Ravazoula, P. Arapantoni Dadioti and G. Nikiforidis, "An image-analysis system based on support vector machines for automatic grade diagnosis of brain-tumourastrocytomass in clinical routine," *Informatics for Health and Social Care*, vol. 30, no. 3, pp. 179-193, 2005.

[9] C. Ortiz De Solorzano, S. Costes, D.E. Callahan, B. Parvin, and M.H. Barcellos Hoff, "Applications of quantitative digital image analysis to breast cancer research," *Microscopy research and technique*, vol. 59, no. 2, pp. 119-127, 2002.

[10] G.A Losa, and C. Castelli, "Nuclear patterns of human breast cancer cells during apoptosis: characterization by fractal dimension and co-occurrence matrix statistics," *Cell and tissue research*, vol. 322, no. 2, pp. 257-267, 2005.

[11] T. Xie, M. Zeidel and Y. Pan, "Detection of tumorigenesis in urinary bladder with optical coherence tomography: optical characterization of morphological changes," *Optics express*, vol. 10, no. 24, pp. 1431-1443, 2002.

[12] E. Vlodavsky, E. Palzur, and J.F. Soustiel, "Hyperbaric oxygen therapy reduces neuro-inflammation and expression of metalloproteinase-9 in rat of traumatic brain injury," *Neuropathology and applied neurobiology*, vol. 32, no. 1, pp. 40-50, 2006.

[13] A.H. Willie, "Cell death: the significance of apoptosis," *Int. Rev. Cytol.*, vol. 68, pp. 251-306, 1980.

[14] M. Ferrari, "Cancer nanotechnology: opportunities and challenges," *Nature Reviews Cancer*, vol. 5, no. 3, pp. 161-171, 2005.

[15] H. Subramanian, P. Pradhan, Y. Liu, I.R. Capoglu, J.D. Rogers, H.K. Roy, R.E. Brand and V. Backman, "Partial-wave microscopic spectroscopy detects Sub-wavelength refractive index fluctuations: an application to cancer diagnosis. *Optics letters*, vol. 34, no. 4, pp. 518-520, 2009.

[16] P. Pradhan, D.Damania, H.M. Joshi, V.Turzhitsky, H. Subramanian, H.K. Roy, A. Taflove, V.P. Dravid and V. Backman, "Quantification of nanoscale density fluctuations using electron microscopy: Light-localization properties of biological cells," *Applied physics letters*, vol. 97, no. 24, pp. 243704, 2010.

[17] M.J. Costello, T.N. Oliver, and L.M. Cobo, "Cellular architecture in age-related human nuclear cataracts," *Investigative Ophthalmology and Visual Science*, vol. 33, pp. 3209-3209, 1992.

[18] J. Cheng andJ.C.Rajapakse, "Segmentation of clustered nuclei with shape markers and marking function," *Biomedical Engineering, IEEE Transactions*, vol. 56, no. 3, pp. 741-748, 2009.

[19] A. Dufour, V. Shinin, S. Tajbakhsh, N. Guillén-Aghion, J.C. Olivo-Marin and C. Zimmer, "Segmenting and tracking fluorescent cells in dynamic 3-Dmicroscopy with coupled active surfaces," *Image Processing, IEEE Transactions*, vol. 14, no. 9, pp. 1396-1410, 2005.

[20] S. John, "Strong localization of photons in certain disordered dielectric super lattices," *Physical review letters*, vol.58, no.23, pp.2486-2489,1987.

[21] J.D. Joannopoulos, P.R. Villeneuve, P. R. and S. Fan, "Photonic crystals: putting a new twist on light," *Nature*, vol. 386, no. 6621, pp.143-149, 1997.

[22] M. Segev, Y. Silberberg and D.N. Christodoulides, "Anderson localization of light," *Nature Photonics*, vol.7, no. 3, pp.197-204, 2013.

[23] World Health Organization (WHO), "*World Health Statistics-2014*" Geneva, Switzerland: World Health organization 2014.

[24] C. Calitz, K.M. Pollack, C. Millard, and D. Yach, "National Institutes of Health Funding for Behavioral Interventions to Prevent Chronic Diseases," *American journal of preventive medicine*, vol. 48, no. 4, pp. 462-471, 2015.

[25] World Health Organization, "World Health Organization global status report on alcohol and health." *Department of Mental Health and Substance Abuse, Geneva* (2014).

[26] R. Siegel, J. Ma, Z. Zou and A. Jemal, "Cancer statistics, 2014. CA," *a cancer journal for clinicians*, vol. 64, no. 1, pp. 9-29, 2014.

[27] A. Berk, and S. L. Zipursky, *Molecular cell biology*, vol. 4, New York: WH Freeman, 2000.

[28] N.ALobo, Y. Shimono, D. Qian and M.F. Clarke, " The biology of cancer stem cells," *Annu. Rev. Cell Dev. Biol.*, vol. 23, pp. 675-699, 2007.

[29] T. Flatscher-Bader, M. Van Der Brug, J.W. Hwang, P.A. Gochee, I. Matsumoto, S.I. Niwa, and P.A. Wilce, "Alcohol-responsive genes in the frontal cortex and nucleusaccumbens of human alcoholics. *Journal of neurochemistry*, vol. 93, no. 2, pp. 359-370, 2005.

[30] E.A Nigg, "Centrosome aberrations: cause or consequence of cancer progression?," *Nature Reviews Cancer*, vol. 2, no. 11, pp. 815-825, 2002.

[31] M. Greaves and C. C. Maley, "Clonal evolution in cancer," *Nature*, vol. 481, no. 7381, pp. 306-313, 2012.

[32] S.D Markowitz and M.M. Bertagnolli, "Molecular basis of colorectal cancer," *New England Journal of Medicine*, vol. 361, no. 25, pp. 2449-2460, 2009.

[33] V. Zappulli, G. De Zan, B. Cardazzo, L. Bargelloni, and M. Castagnaro, "Feline mammary tumours in comparative oncology," *Journal of dairy research*, vol. 72, no. S1, pp. 98-106, 2005.

[34] A.I Baba and C. Câtoi, *Comparative oncology*, The publishing house of the Romanian Academy, 2007.

[35] M.C. Paoloni, M. C. and C. Khanna, "Comparative oncology today," *Veterinary Clinics of North America: Small Animal Practice*, vol.*37*, no.6, pp.1023-1032, 2007.

[36] P. Pradhan, D. Damania, H.M. Joshi, V. Turzhitsky, H. Subramanian, H.K. Roy, A. Taflove, V.P. Dravid and V. Backman, "Quantification of nanoscale density fluctuations by electron microscopy: probing cellular alterations in early carcinogenesis," *Physical biology*, vol. 8, no. 2, pp.026012-026021, 2011.

[37] B. Miller, *Cancer: We Can Win The War Against Cancer By Aggresively pursuing Prevention*. Oak Publication SdnBhd, 2005.

[38] E. Giovannucci, M.J. Stampfer, G.A. Colditz, E.B. Rimm, D. Trichopoulos, B.A. Rosner, F.E. Speizer and W.C. Willett, " Folate, methionine, and alcohol intake and risk of colorectal adenoma," *Journal of the National Cancer Institute*, vol. 85, no. 11, pp. 875-883, 1993.

[39] Y.I. Kim, "Role of folate in colon cancer development and progression," *The Journal of nutrition*, vol. 133, no. 11, pp. 3731S-3739S, 2003.

[40] R. H. Johnson, G. Eisenhofer and D.G. Lambie, "The effects of acute and chronic ingestion of ethanol on the autonomic nervous system," *Drug and alcohol dependence*, vol.18, no.4, pp.319-328.

[41] M.D. De Bellis, D.B. Clark, S.R. Beers, P.H. Soloff, A.M. Boring,J. Hall, A. Kersh and M.S. Keshavan, "Hippocampal volume in adolescent-onset alcohol use disorders," *American Journal of Psychiatry*, vol. 157, no. 5, pp. 737-744, 2000.

[42] T.P. Beresford, D.B. Arciniegas, J. Alfers, L. Clapp, B. Martin, Y. Du, D. Liu, D. Shen and C. Davatzikos, "Hippocampus volume loss due to chronic heavy drinking," *Alcoholism: Clinical and Experimental Research*, vol. 30, no. 11, pp. 1866-1870, 2006.

[43] D.M. Bannerman, J.N.P. Rawlins, S.B. McHugh, R.M.J. Deacon, B. K.Yee, T. Bast, W N Zang, H.H.J. Pothiuizen and J. Feldon, "Regional dissociations within the hippocampus memory and anxiety," *Neuroscience &Biobehavioral Reviews*, vol. 28, no. 3, pp. 273-283, 2004.

[44] J.A King, I. Trinkler, T. Hartley, F. Vargha-Khadem, and N. Burgess, "The Hippocampal Role in Spatial Memory and the Familiarity-Recollection Distinction: A Case Study," *Neuropsychology*, vol.18, no. 3, pp. 405-417, 2004.

[45] B.S McEwen, "Mood disorders and allostatic load," *Biological psychiatry*, vol. 54, no. 3, pp. 200-207,2003.

[46] K.I. Erickson, R.S. Prakash, M.W. Voss, L. Chaddock, L. Hu, K.S. Morris, S.M. White, T.R. Wójcicki, E. McAuley, and A.F. Kramer, "Aerobic fitness is associated with hippocampal volume in elderly humans," *Hippocampus*, vol. 19, no. 10, pp. 1030-1039, 2009.

[47] Y. Nishii, M. Yamaguchi, Y. Kimura, T. Hasegawa, H. Aburatani, H. Uchida, K. Hirata, and Y. Sakuma, "A newly developed anti-Mucin 13 monoclonal antibody targets pancreatic ductal adenocarcinoma cells," *International journal of oncology*, vol. 46, no. 4, pp. 1781-1787, 2015.

[48] P. Boffetta and M. Hashibe, " Alcohol and cancer," *The lancet oncology*, vol. 7, no. 2, pp. 149-156, 2006.

[49] T. Babor, "*Alcohol: no ordinary commodity: research and public policy,*" Oxford University Press, 2010.

[50] B.Sadikovic, K. Al-Romaih, J.A Squire, and M.Zielenska, "Cause and consequences of genetic and epigenetic alterations in human cancer," *Current genomics*, vol. 9, no.6, pp. 394-408, 2008.

[51] D.L. Topping, and P.M. Clifton, "Short-chain fatty acids and human colonic function: roles of resistant starch and nonstarch polysaccharides.*Physiological reviews*, vol. 81, no.3, pp.1031-1064, 2001.

[52] L. Shen, M. Toyota, Y. Kondo, E. Lin, L. Zhang, Y.Guo, N.S. Hernandez and J.P.J. Issa, "Integrated genetic and epigenetic analysis identifies three different subclasses of colon cancer," *Proceedings of the National Academy of Sciences*, vol. 104, no. 47, pp. 18654-18659, 2007.

[53] J.N. Riley andD.W. Walker, "Morphological alterations in hippocampus after long-term alcohol consumption in mice," *Science*, vol. 201, no. 4356, pp. 646-648, 1978.

[54] S. Khan, M.C. Ebeling, M.S. Zaman, M.Sikander, M. Yallapu, N. Chauhan, A. Y. Yacoubian and S.C. Chauhan"MicroRNA-145 targets MUC13 and suppresses growth and invasion of pancreatic cancer," *Oncotarget*, vol. 5, no. 17, 7599.

[55] C. A. O'Brien, A. Pollett, S.Gallinger, J.E. Dick, "A human colon cancer cell capable of initiating tumor growth in immune-deficient mice," *Nature*, vol. 445, no. 7123, pp. 106-110, 2007.

[56] K. Aoki, T. Yoshida, N. Matsumoto, H. Ide, T. Sugimura and M. Terada, "Suppression of Ki-ras p21 levels leading to growth inhibition of pancreatic cancer cell lines with Ki-ras mutation but not those without Ki-ras mutation," *Molecular carcinogenesis*, vol. 20, no. 2, pp. 251-258, 1997.

[57] Y. Li, K.L. Ellis, S. Ali, B.F. El-Rayes, A. Nedeljkovic-Kurepa, O. Kucuk, P.A. Philip, and F.H. Sarkar, " Apoptosis-inducing effect of chemotherapeutic agents is potentiated by soy isoflavonegenistein, a natural inhibitor of NF-κB in BxPC-3 pancreatic cancer cell line," *Pancreas*, vol. 28, no.4, pp. e90-e95, 2004.

[58] M. Lieber, J. Mazzetta, W. Nelson-Rees, M. Kaplan, and G.Todaro, "Establishment of a continuous tumor? cell line (PANC? 1) from a human Carcinomaof the exocrine pancreas," *International journal of cancer*, vol. 15, no. 5, pp. 741-747, 1975.

[59] X.Z. Ding, W.G. Tong, and T.E Adrian, "Blockade of cyclooxygenase-2 inhibits proliferation and induces apoptosis in human pancreatic cancer cells," *Anticancer research*, vol. 20, no. 4, pp. 2625-2631, 1999.

[60] D.B. Williams, and C.B.Carter,*The transmission electron microscope* Springer Us 1996.

[61] L. Reimer, *Transmission electron microscopy: physics of image formation and microanalysis*, vol. 36, Springer 2013.

[62] D.E. Caldwell, D.R. Korber, and J.R. Lawrence, Confocal laser microscopy and digital image analysis in microbial ecology. In *Advances in microbial ecology*, pp. 1-67, Springer US.1992

[63] J. Vörös, "The density and refractive index of adsorbing protein layers," *Biophysical journal*, vol. 87, no. 1, pp. 553-561, 2004.

[64] P. Wang, R.K.Bista, W.Qiu, W.E. Khalbuss, L. Zhang, R.E. Brand, and Y. Liu, "An insight into statistical refractive index properties of cell internal structure via low-coherence statistical amplitude microscopy," *Optics express*, vol. 18, no. 21, pp. 21950-21958, 2010.

[65] Z.L. Wang, "Transmission electron microscopy of shape-controllednanocrystals and their assemblies," *The Journal of Physical Chemistry B*, vol. 104, no. 6, pp. 1153-1175.

[66] J. Goldstein, D.E. Newbury, P.Echlin,D. C. Joy, Jr. A.D. Romig , C.E. Lyman, C. Fiori and E. Lifshin," *Scanning electron microscopy and X-ray microanalysis: a text for biologists, materials scientists, and geologists*" Springer Science & Business Media, 2012.

[67] S. Reich, J. Maultzsch, C. Thomsen and P. Ordejon,"Tight-binding description of graphene," *Physical Review B*, vol. 66, no. 3, pp. 035412, 2002.

[68] E.N.E.E. Lidorikis, M.M. Sigalas, E.N. Economou, and C.M. Soukoulis, "Tight-binding parametrization for photonic band gap materials," *Physical review letters*, vol. 81, no. 7, pp. 1405, 1998.

[69] F. Wegner, "Inverse participation ratio in 2+ ε dimensions", *Zeitschriftfür Physik B Condensed Matter*, vol. 36, no. 3, pp. 209-214, 1980.